Lecture 29:
The End Stages of Massive Stellar Evolution & Supernova

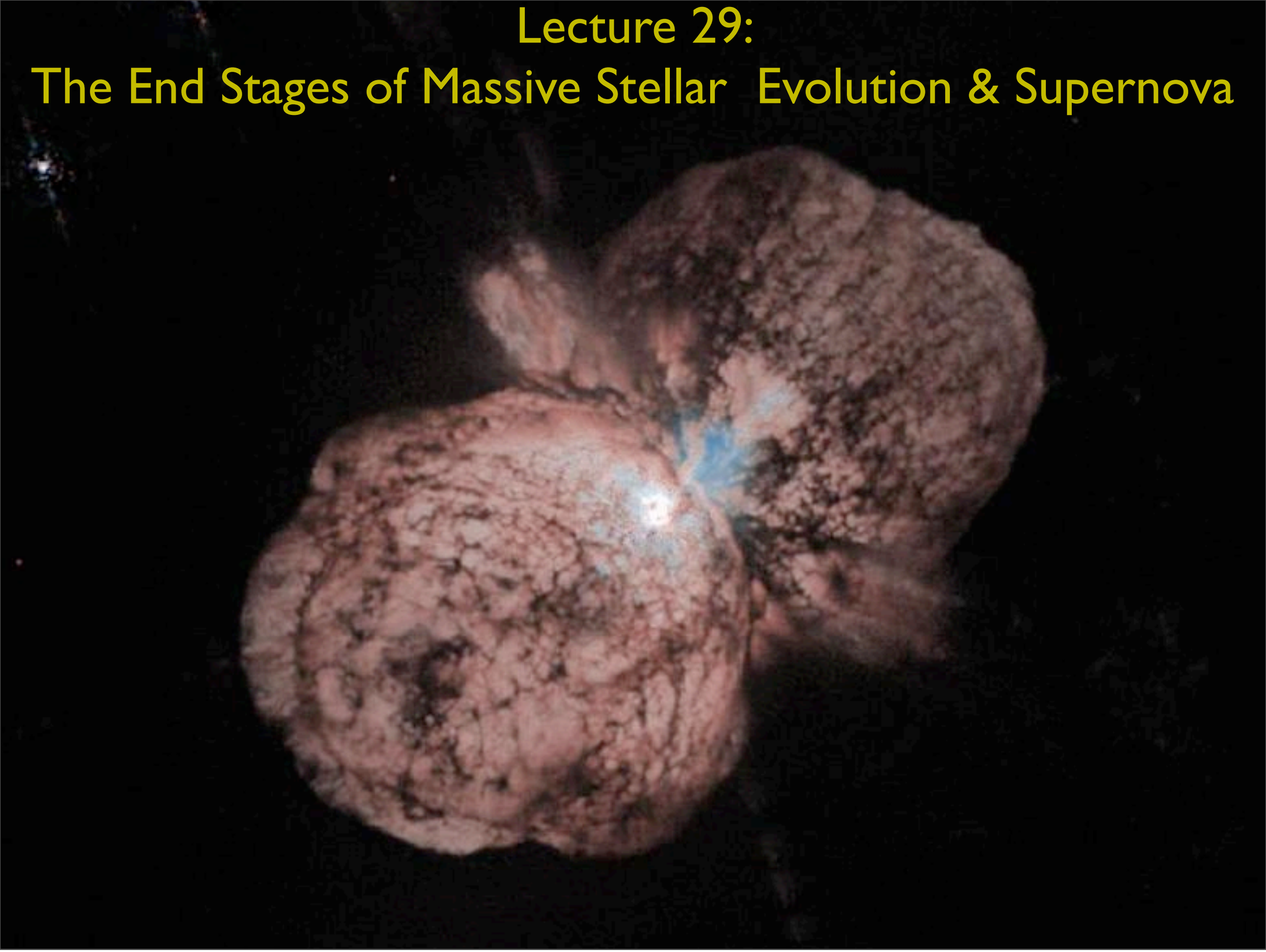

Review: Elemental Abundances in the Solar System

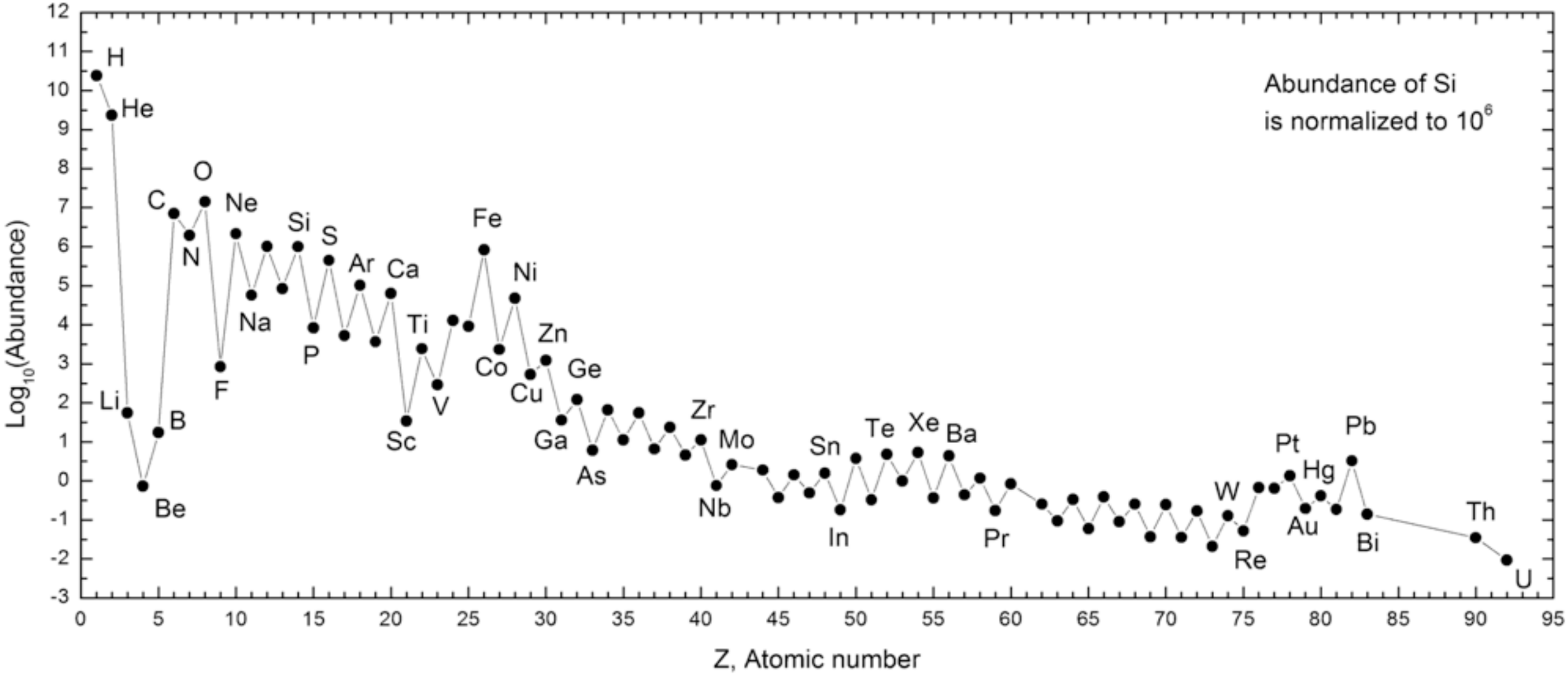

Review: Elemental Abundances in the Solar System

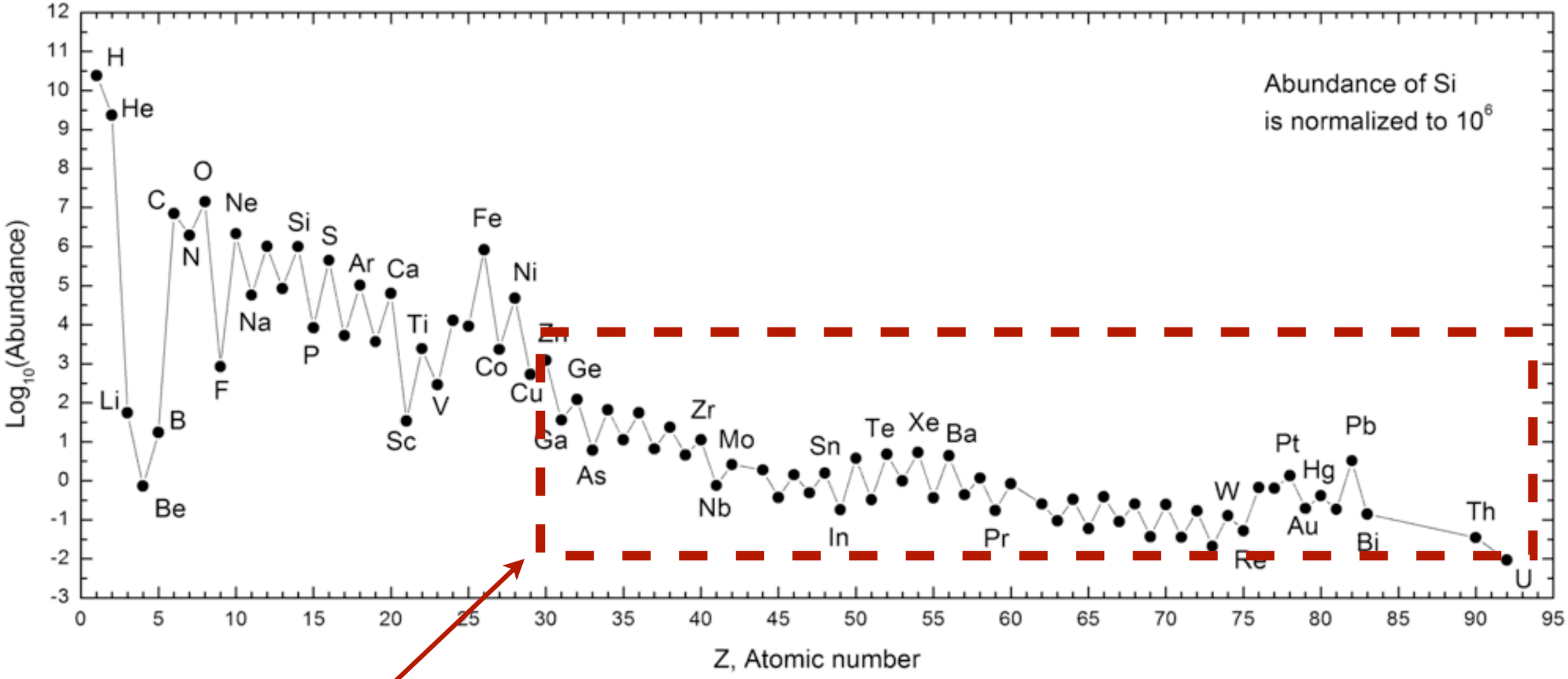

Synthesized by S and R-processes

Review: Elemental Abundances in the Solar System

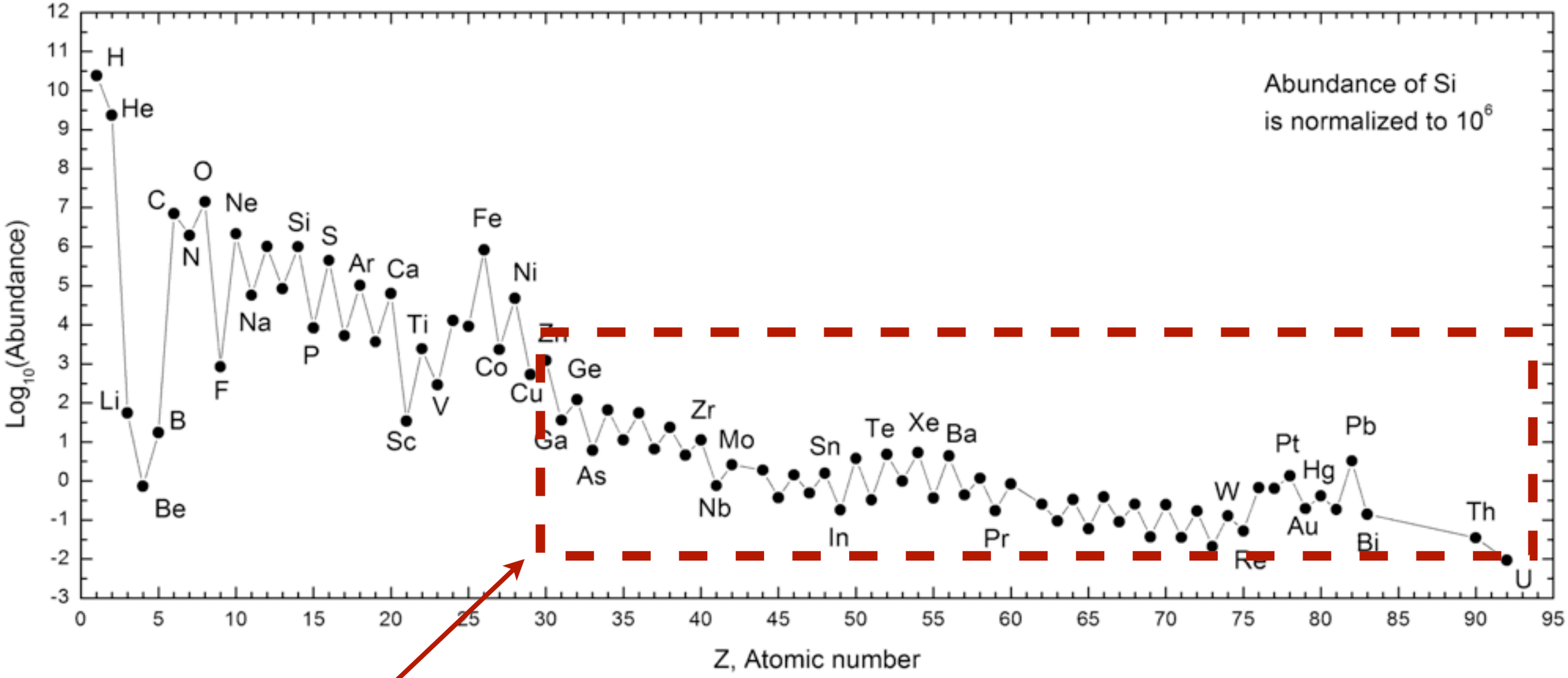

Synthesized by S and R-processes

What causes all the structure?

Dominant Elements in Nuclear Statistical Equilibrium

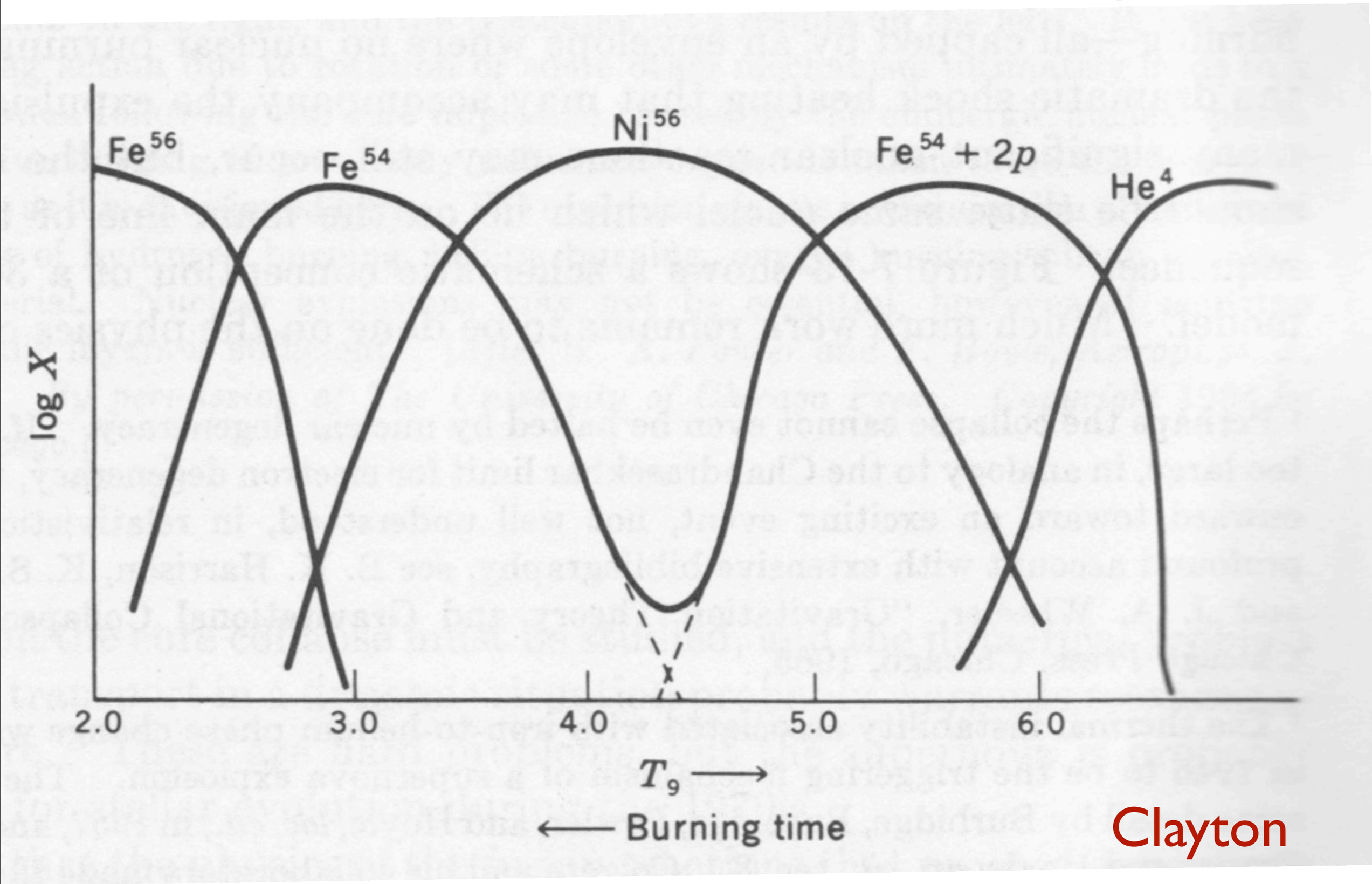

Clayton

the s-process

Clayton

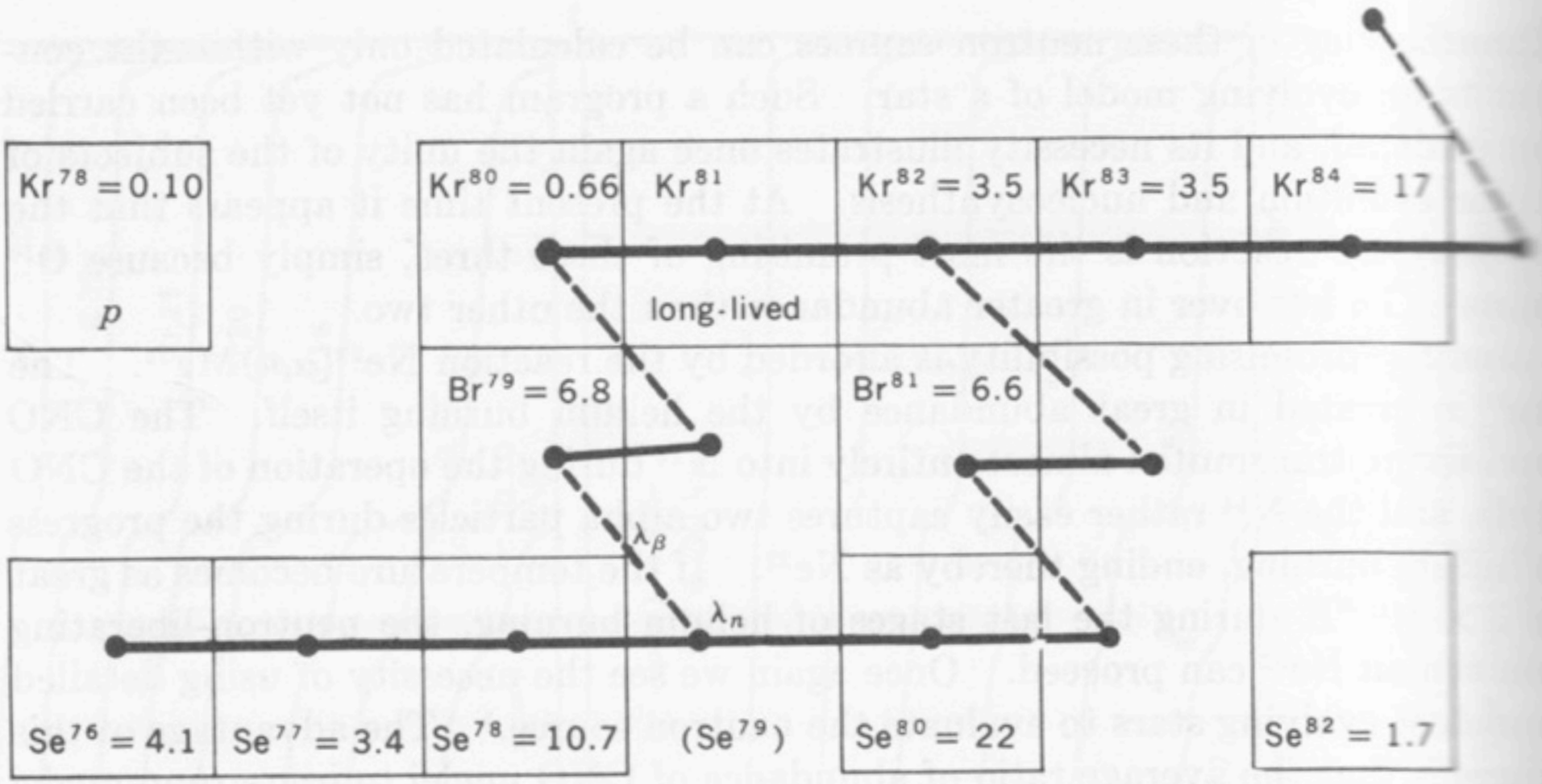

Fig. 7-26 The *s*-process path through selenium, bromine, and krypton. An interesting branch between neutron capture and beta decay occurs at Se^{79}, which has a laboratory half-life of 6.5×10^4 years. Both Kr^{80} and Kr^{82} are shielded from *r*-process production, by Se^{80} and Se^{82}, respectively. The ratio of *s*-process current through Kr^{80} to that through Kr^{82} is equal to the ratio of $\lambda_\beta(Se^{79})$ to $\lambda_\beta(Se^{79}) + \lambda_n(Se^{79})$. The abundance of each nucleus per 10^6 silicon atoms in the solar system is indicated.

The s-processes produces stable nuclei where Z ~ N

Cross Section to Neutron Capture

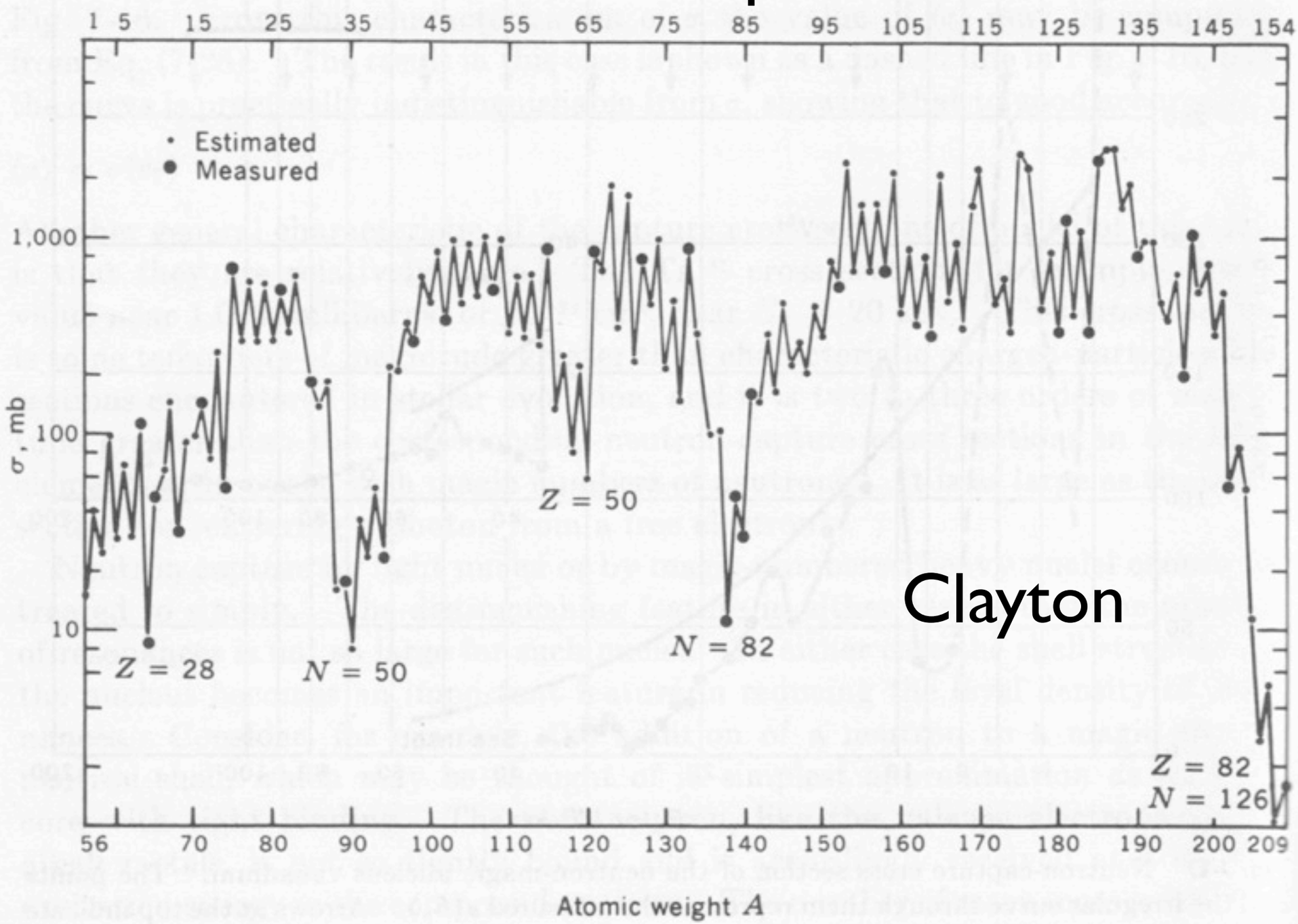

Clayton

Fig. 7-18 Measured and estimated neutron-capture cross sections of nuclei on the *s*-process path. The neutron energy is near 25 kev. The cross sections show a strong odd-even effect reflecting average level densities in the compound nucleus. Even more obvious is the strong influence of the closed nuclear shells, or magic numbers, which are associated with precipitous drops in the cross section. Nucleosynthesis of the *s*-process nuclei is dominated by the small cross sections of the neutron-magic nuclei.

S-process abundances

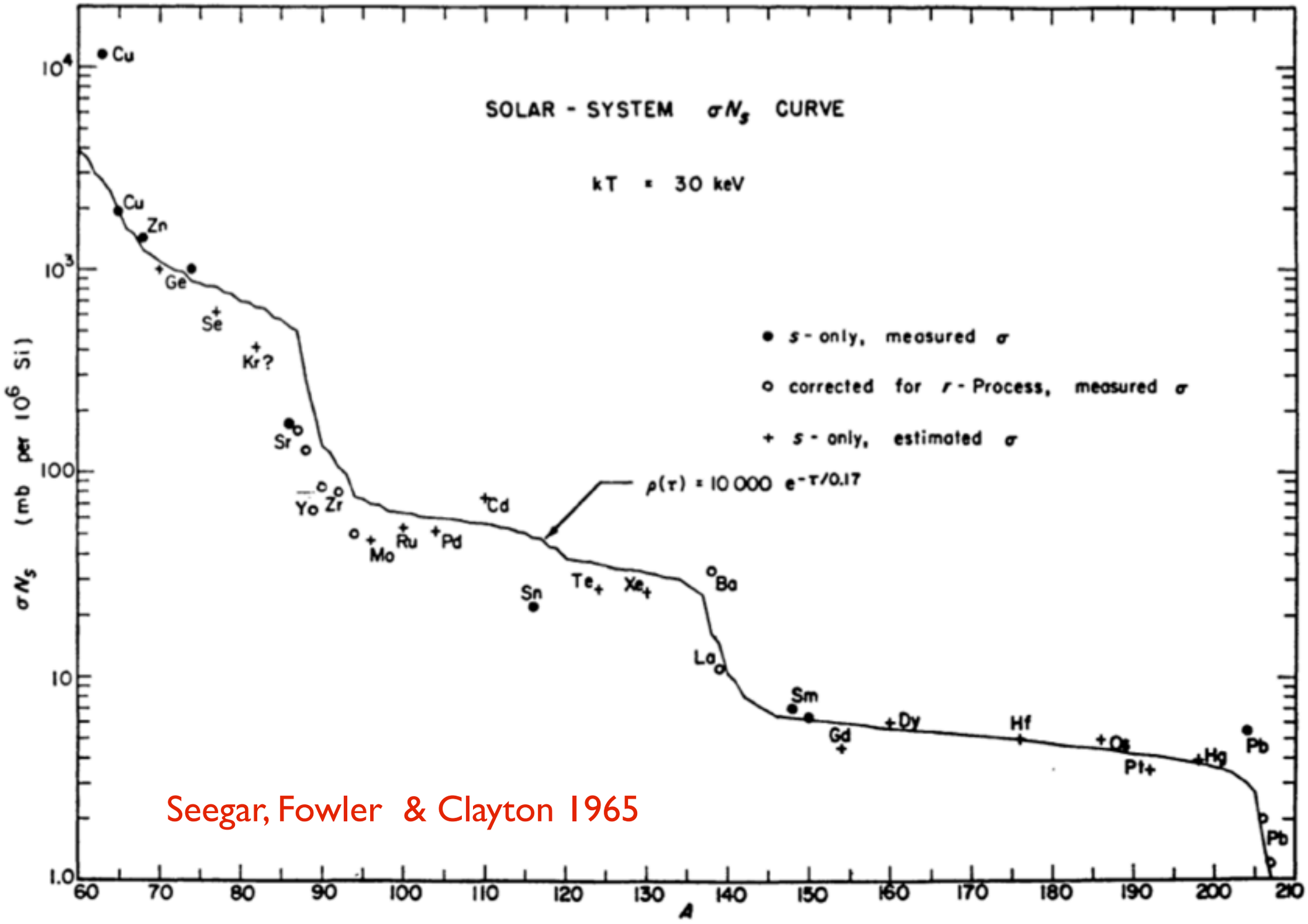

Seegar, Fowler & Clayton 1965

FIG. 1.—Solar-system σN_s-curve. The product of the neutron-capture cross-section at $kT = 30$ keV (in mb) times isotopic abundance (Si = 10^6) is plotted versus atomic mass number A. The solid line is a calculated curve corresponding to an exponential distribution of integrated neutron flux.

The points are the neutron cross-section x the solar system abundance. This varies smoothly with atomic weight. The line is the theoretical prediction calculated assuming an exponential distribution of neutron exposures.

the s and r-processes

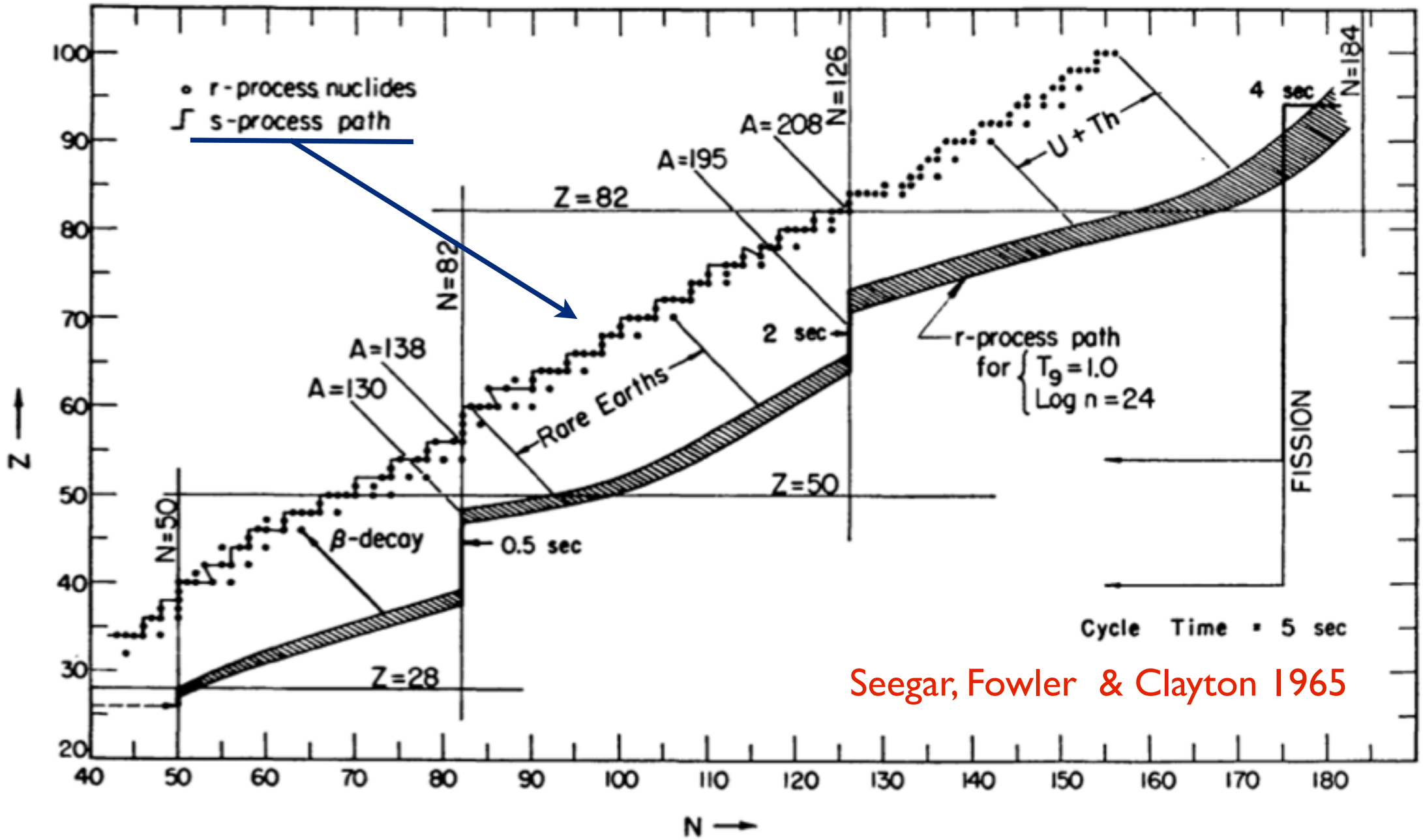

Seegar, Fowler & Clayton 1965

FIG. 10.—Neutron-capture paths. The *s*-process follows a path in the *N*–*Z*-plane which is near the line of beta-stability, and is represented by the single line. The *r*-process progenitor nuclei occupy a band in the neutron-rich area of the *N*–*Z*-plane, such as the shaded area here (calculated for $T_9 = 1.0$, log $n_n = 24$). Subsequently the progenitors beta-decay to the stable nuclei represented by circles; in many cases these end products of the *r*-process are also produced in the *s*-process. The observed abun dance peaks at $A = 130$ and $A = 138$ are attributed to the magic neutron number 82, and the peaks at $A = 195$ and $A = 208$ to $N = 126$. As neutrons are captured in the *r*-process, material starting at $Z = 26$ in the lower left-hand corner moves up the shaded band, reaching the $A \sim 130$ peak 0.5 sec and the $A \sim 195$ peak 2 sec after starting. After 4 sec material begins to reach $Z = 94$, where neutron-induced fission occurs; then a cyclic situation is established, and the number of nuclei is doubled by fission every 5 sec.

the r-process elements

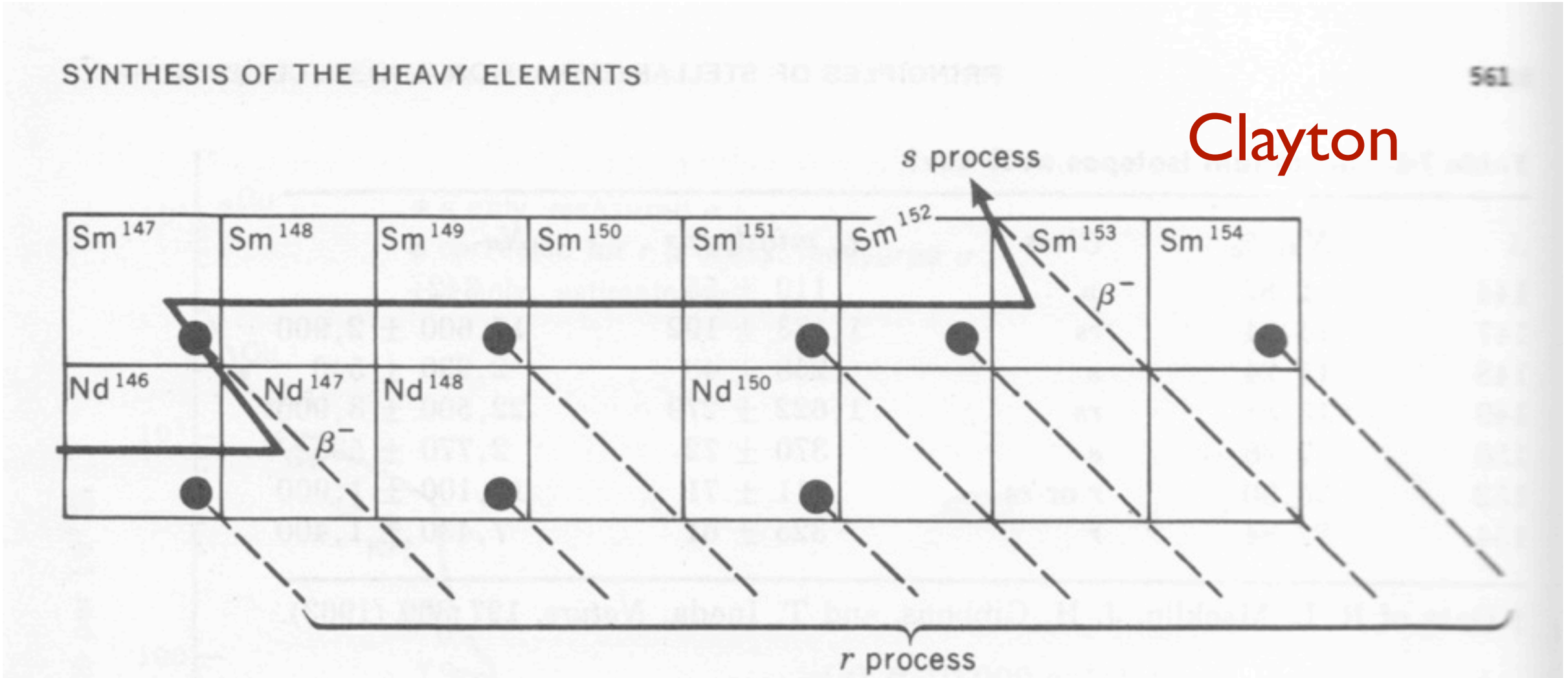

Fig. 7-19 The *s*-process path through the isotopes of samarium. The *r*-process yield contributes to the abundances of the nuclei containing the solid dots. Two of the isotopes of samarium, Sm^{148} and Sm^{150}, are *s*-only nuclei.

The r-process elements are created when the neutron rich elements undergo beta decay.

The r-process

Seegar, Fowler & Clayton 1965

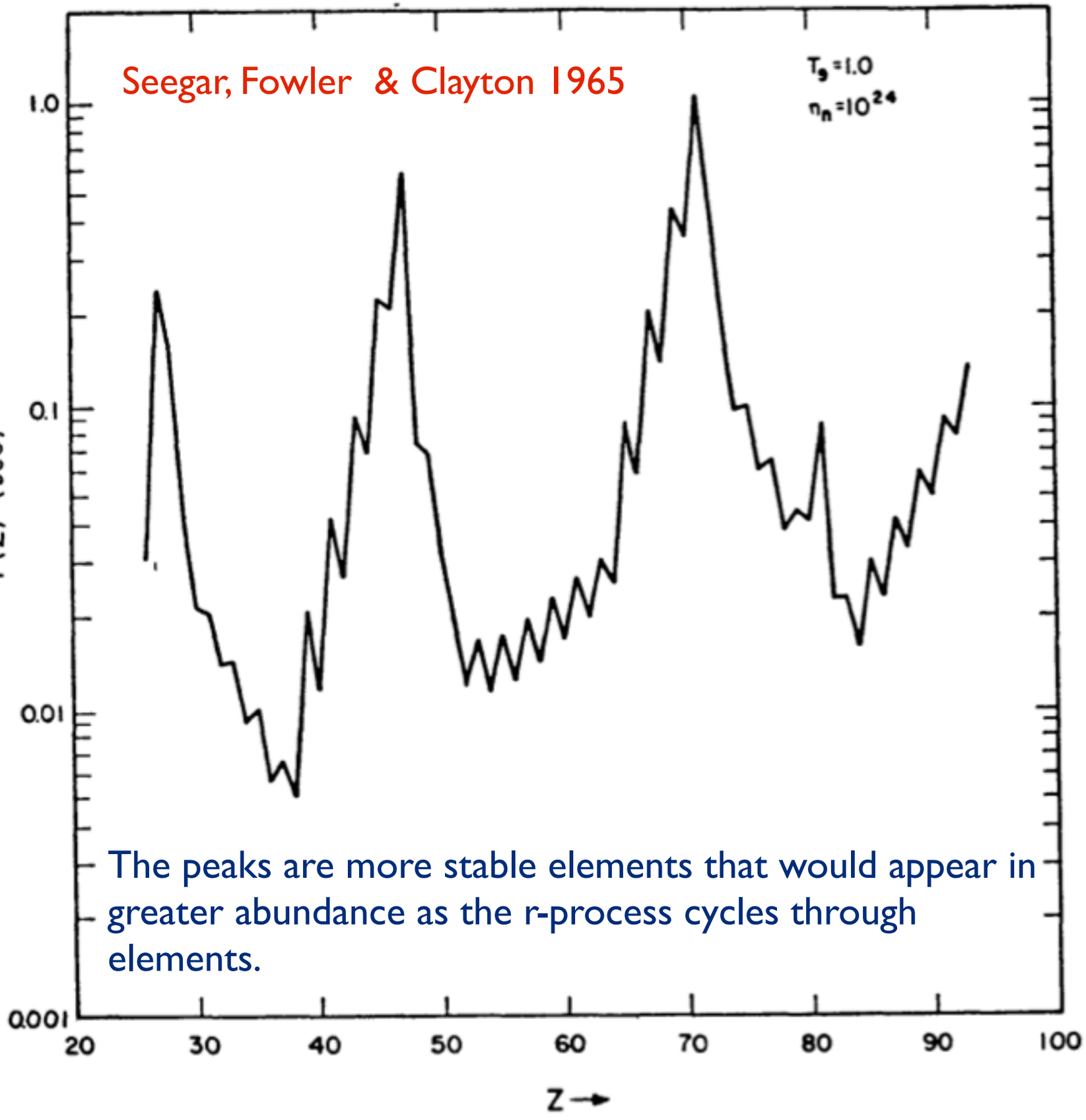

The peaks are more stable elements that would appear in greater abundance as the r-process cycles through elements.

FIG. 11.—Beta-decay mean life. The mean life for beta-decay of the isotopes of each Z is plotted versus Z.

the r-process predicted abundances

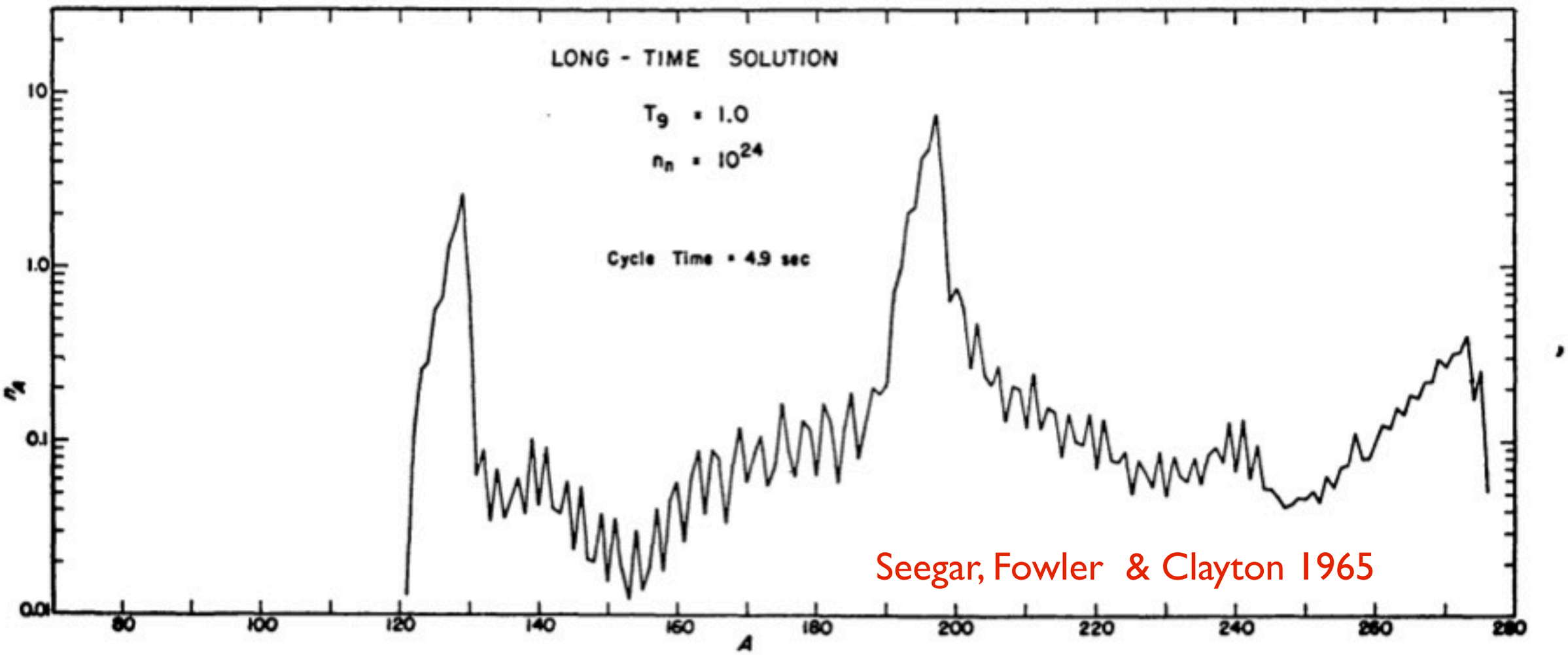

FIG. 13

As the r-process cycles through the elements (every 5 seconds in the above models), the above abundance distribution will be established. The abundances will double every cycle. Peaks are due to stable nuclei.

r-process abundances

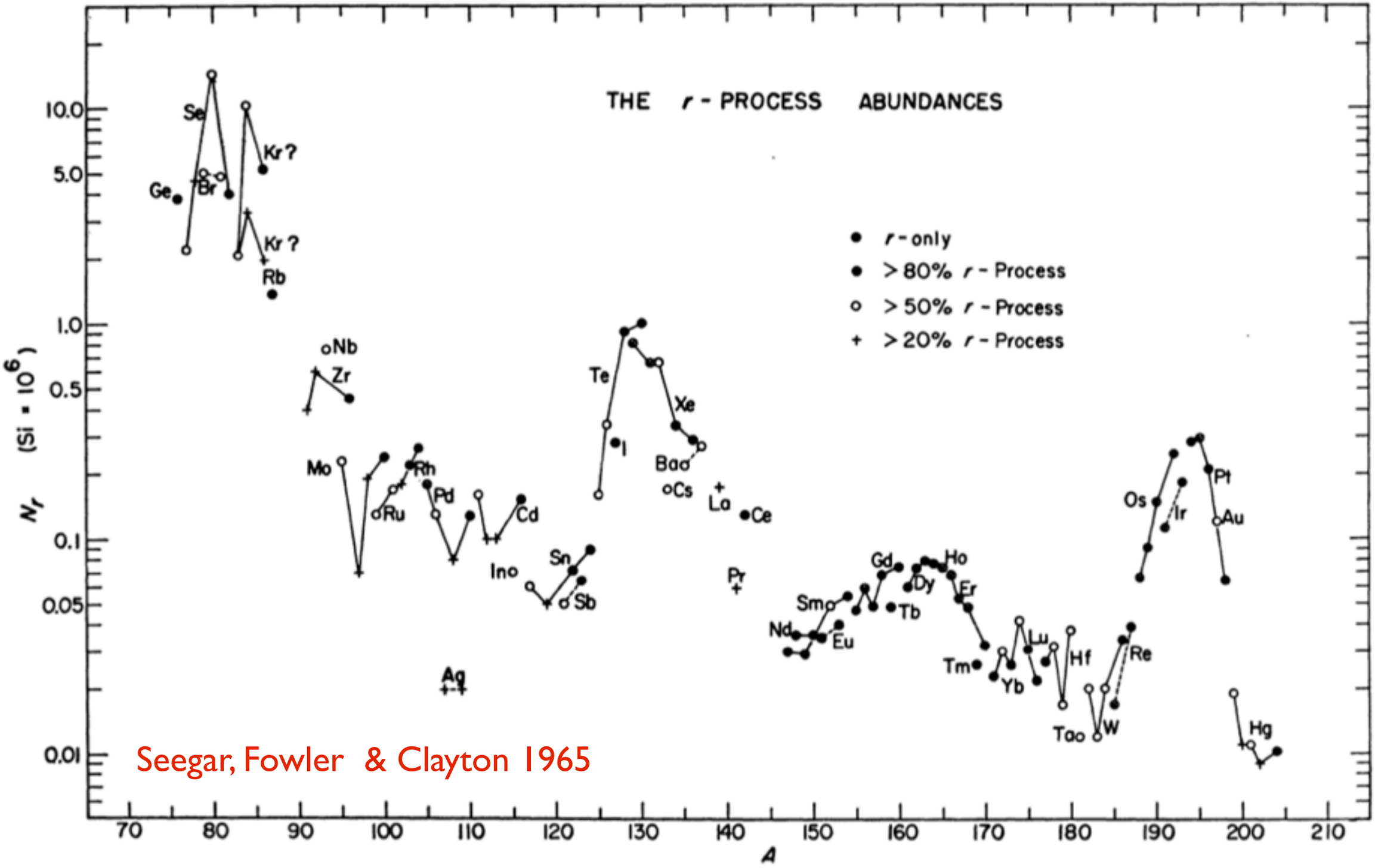

Seegar, Fowler & Clayton 1965

FIG. 6.—Solar-system *r*-process abundances. Abundances of isotopes produced in the *r*-process are plotted after subtraction of the contribution by the *s*-process. Isotopes of a given element are joined by lines (solid line = even *Z*, dashed line = odd *Z*). The ambiguity at Kr is discussed in the text.

These are R-process abundances after the subtraction of the S-process abundances

Massive Star Evolution

1990A&AS..

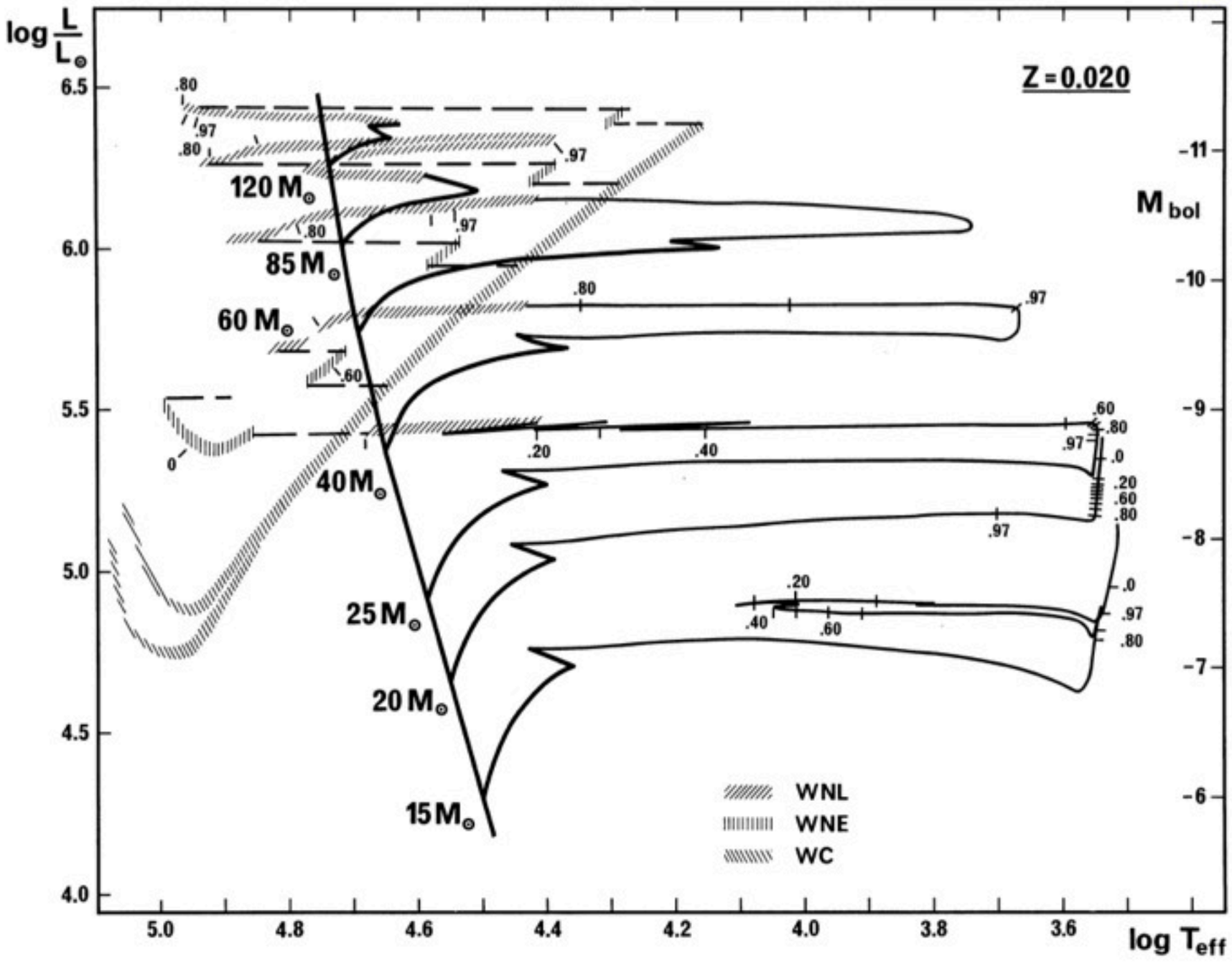

$$\frac{L_{edd}}{M} = \frac{4\pi G m_H c}{\sigma_T} = 3.2 \times 10^4 \frac{L_\odot}{M_\odot}$$

Maeder et al. 1990 A&AS 84, 139

Wolf Rayet Stars: Massive Blue Stars with Strong Line Emission

WN: HeII and N lines
WNha: HeII, N and H lines
WC & WO: HeII, C and O lines

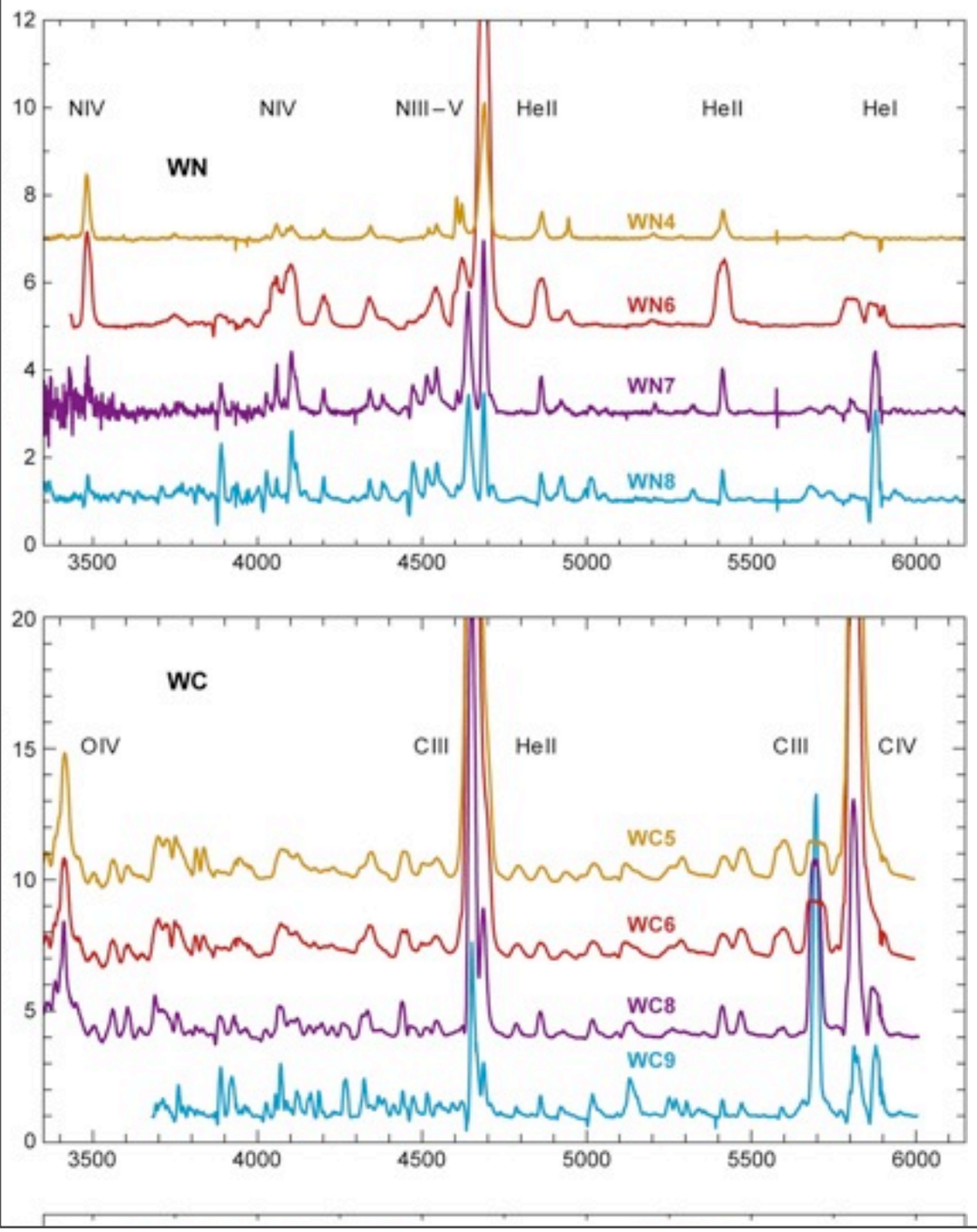

Table 2 Physical and wind properties of Milky Way WR stars (LMC in parenthesis)

Sp	T_*	log L	$\dot{M}$	v_∞	log N(LyC)	M_v	Example
Type	kK	$L_\odot$	$M_\odot$ yr^{-1}	km s^{-1}	ph s^{-1}	mag	
WN stars							
3-w	85	5.34	–5.3	2200	49.2	–3.1	WR3
4-s	85	5.3	–4.9	1800	49.2	–4.0	WR6
5-w	60	5.2	–5.2	1500	49.0	–4.0	WR61
6-s	70	5.2	–4.8	1800	49.1	–4.1	WR134
7	50	5.54	–4.8	1300	49.4	–5.4	WR84
8	45	5.38	–4.7	1000	49.1	–5.5	WR40
9	32	5.7	–4.8	700	48.9	–6.7	WR105
WNha stars							
6ha	45	6.18	–5.0	2500	49.9	–6.8	WR24
9ha	35	5.86	–4.8	1300	49.4	–7.1	WR108
WC and WO stars							
(WO)	(150)	(5.22)	(–5.0)	(4100)	(49.0)	(–2.8)	(BAT123)
(4)	(90)	(5.54)	(–4.6)	(2750)	(49.4)	(–4.5)	(BAT52)
5	85	5.1	–4.9	2200	48.9	–3.6	WR111
6	80	5.06	–4.9	2200	48.9	–3.6	WR154
7	75	5.34	–4.7	2200	49.1	–4.5	WR90
8	65	5.14	–5.0	1700	49.0	–4.0	WR135
9	50	4.94	–5.0	1200	48.6	–4.6	WR103

Note: Data adapted from Herald, Hillier & Schulte-Ladbeck (2001) and Hamann, Gräfener & Liermann (2006) for WN stars; and from Barniske, Hamann & Gräfener (2006) and Crowther et al. (2002, 2006a, and references therein) for WC stars. Abundances are shown by mass fraction in percent. Mass-loss rates assume a volume filling factor of $f = 0.1$.

Crowther et al. 2007

Luminous Blue Variables

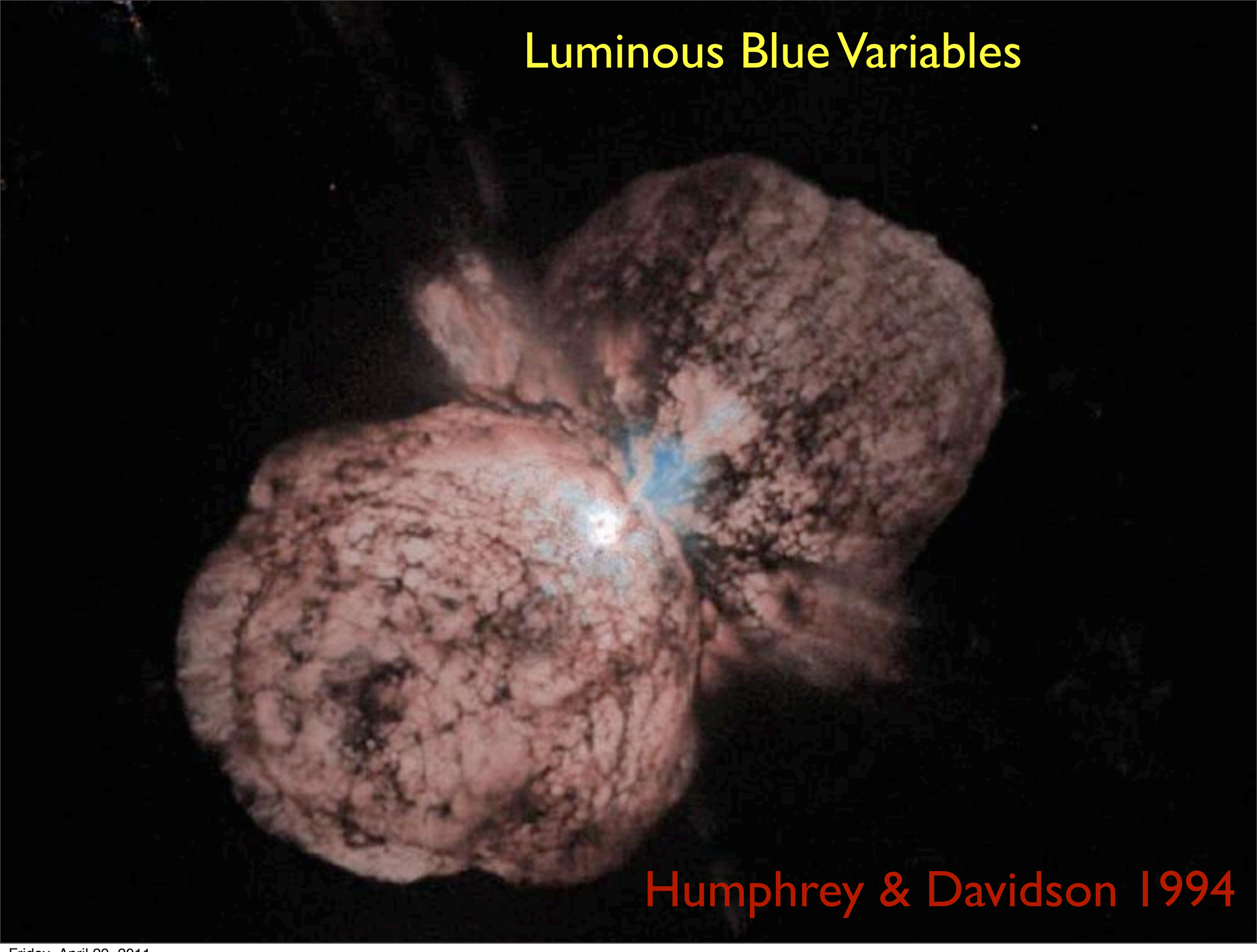

Humphrey & Davidson 1994

Luminous Blue Variables

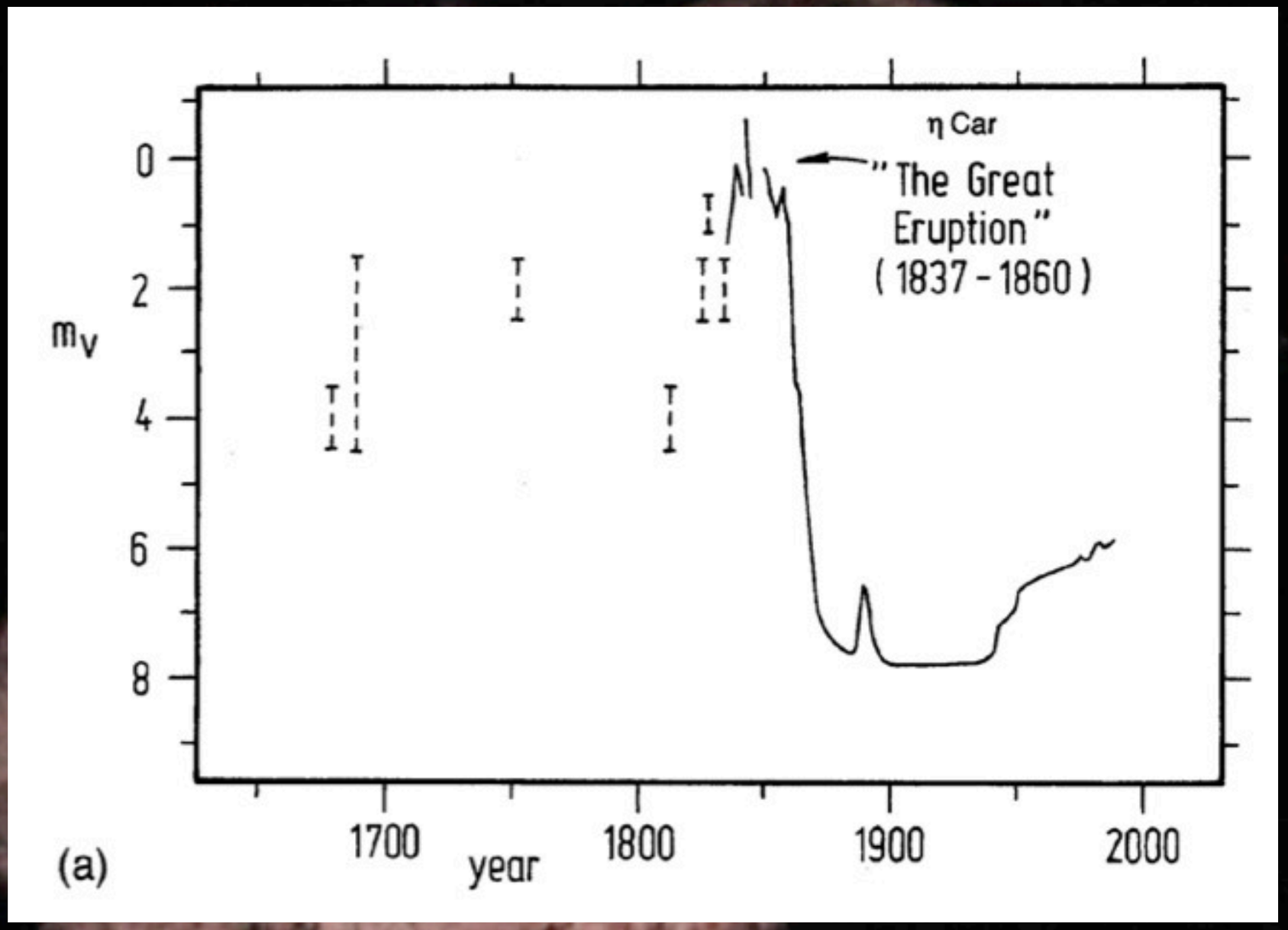

Humphrey & Davidson 1994

Luminous Blue Variables, Hypergiants, and Red Supergiants

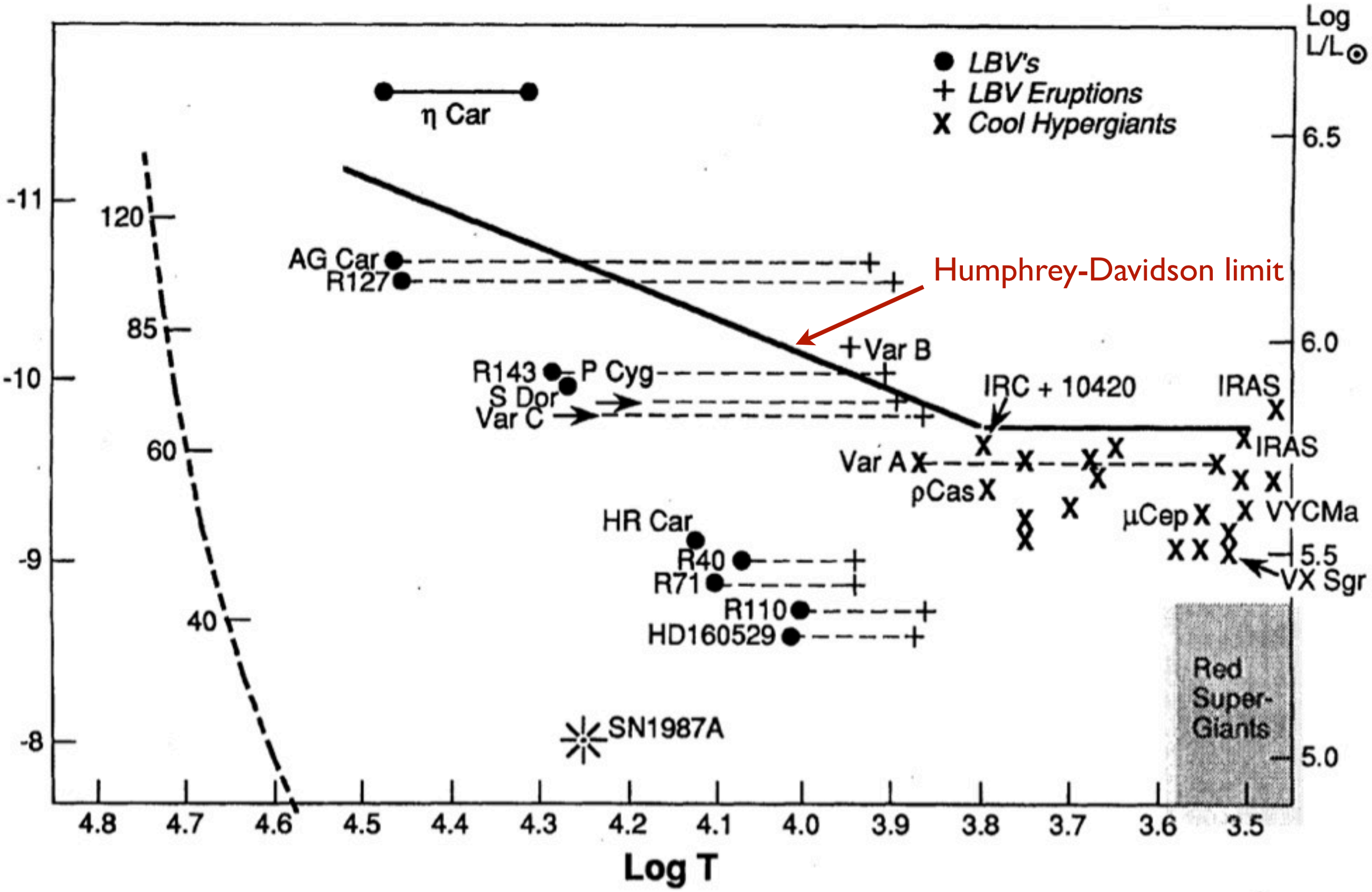

Humphrey & Davidson 1994

Evolution of Central Temperatures and Densites

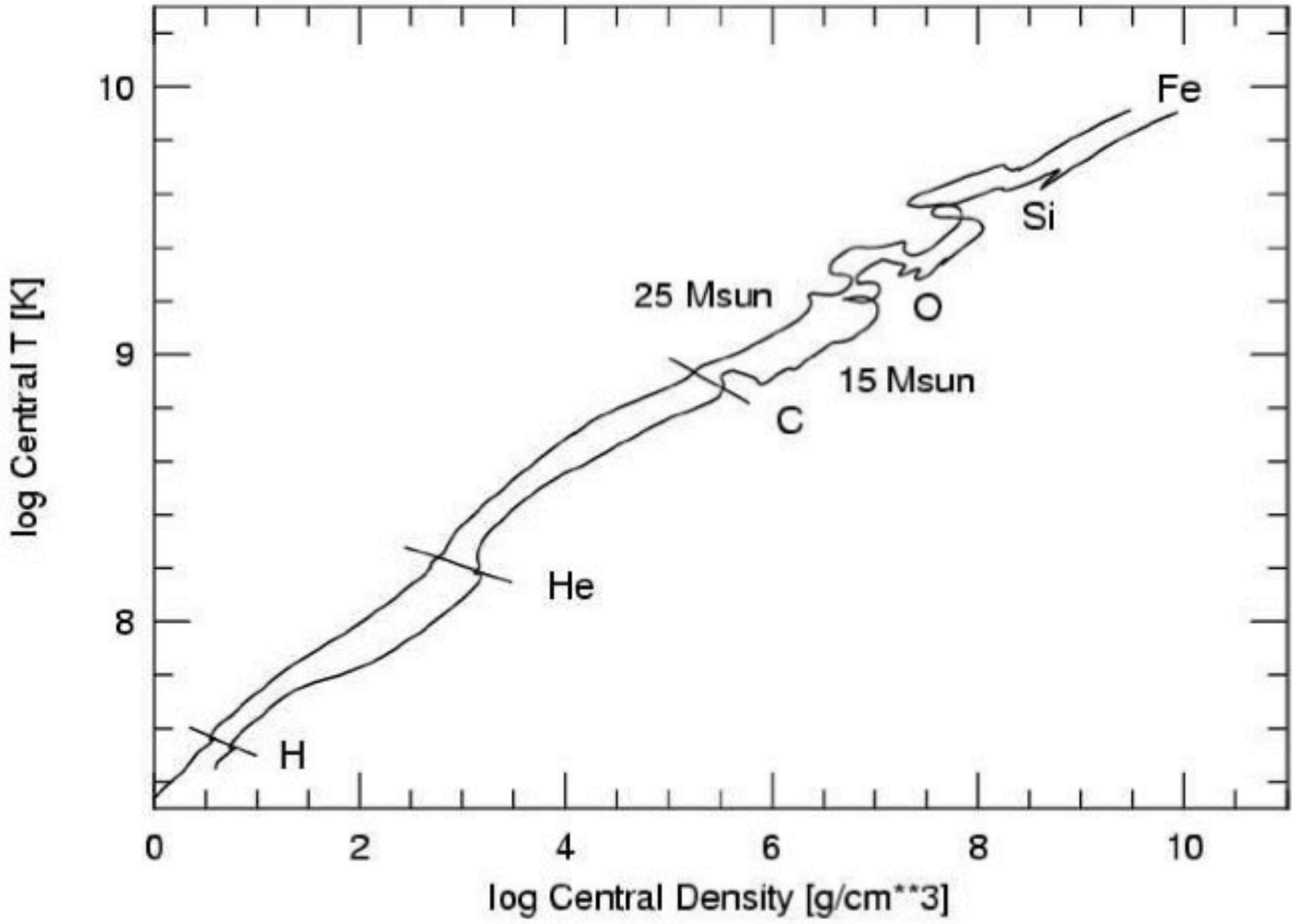

Figure 1: *The evolution of the temperature and density for the centre of two massive stars, 15 and 25 times heavier than the Sun. Labels show the location where the star pauses to burn a given fuel (Table 1). Overall, the evolution of a massive star is a continued contraction to higher density and temperature, a contraction that only ends when a neutron star or black hole is formed. During most of the evolution the density is proportional to the cube of the temperature, as expected for an ideal gas in hydrostatic equilibrium, but there are deviations caused by nuclear burning and the partial quantum mechanical degeneracy of the electrons.*

Woosley and Janka 2005

Elemental Abundances Before a Supernova

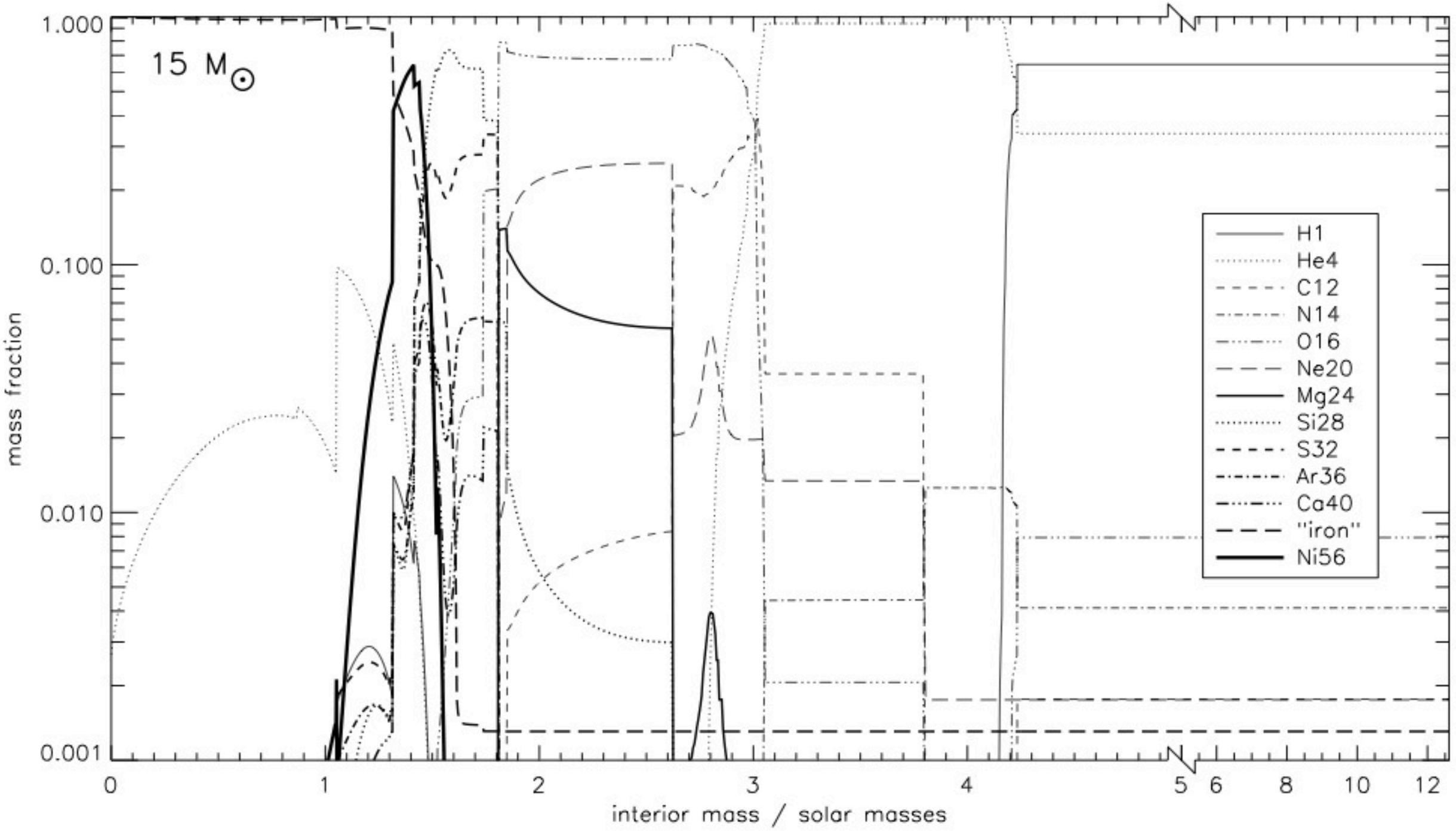

Woosley, Heager & Weaver 2002

Core Collapse

Driven by pressure drops due to loss of energy by neutrinos, photodisintegration and capture of e^- by protons, core contracts.

Mass exceeds the Chandresekhar mass.

Velocities reach about 1/4 c

Collapse from size of Earth to 30 km in
~ 1 s

Collapse stops when density approach 4-5x10^{14} gm cm^{-3} and nuclear repulsion forces become dominant.

Infall velocity in presupernova

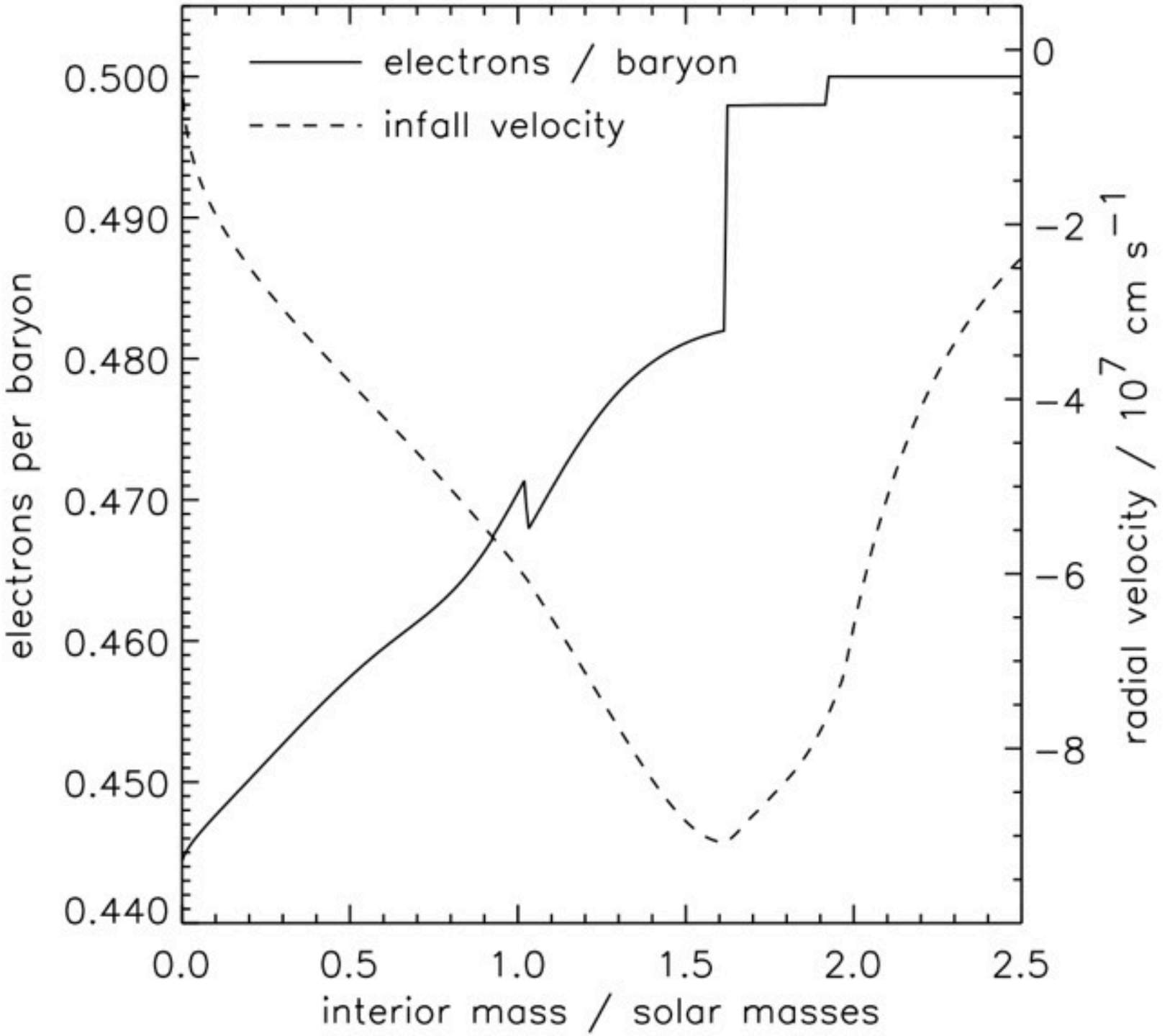

FIG. 18: Distribution of Y_e (solid) and collapse velocity (dashed) in the inner 2.5 $M_\odot$ of a 15 $M_\odot$ presupernova star.

Woosley, Heager & Weaver 2002

The Bounce

The abrupt stop of collapse (by nuclear repulsive forces) creates a bounce.

Bounce stalls quickly due to energy losses (neutrinos and photodisintegration).

After bounce, core accreting matter at a few solar masses per second. If this last for even one second, core would collapse into black hole.

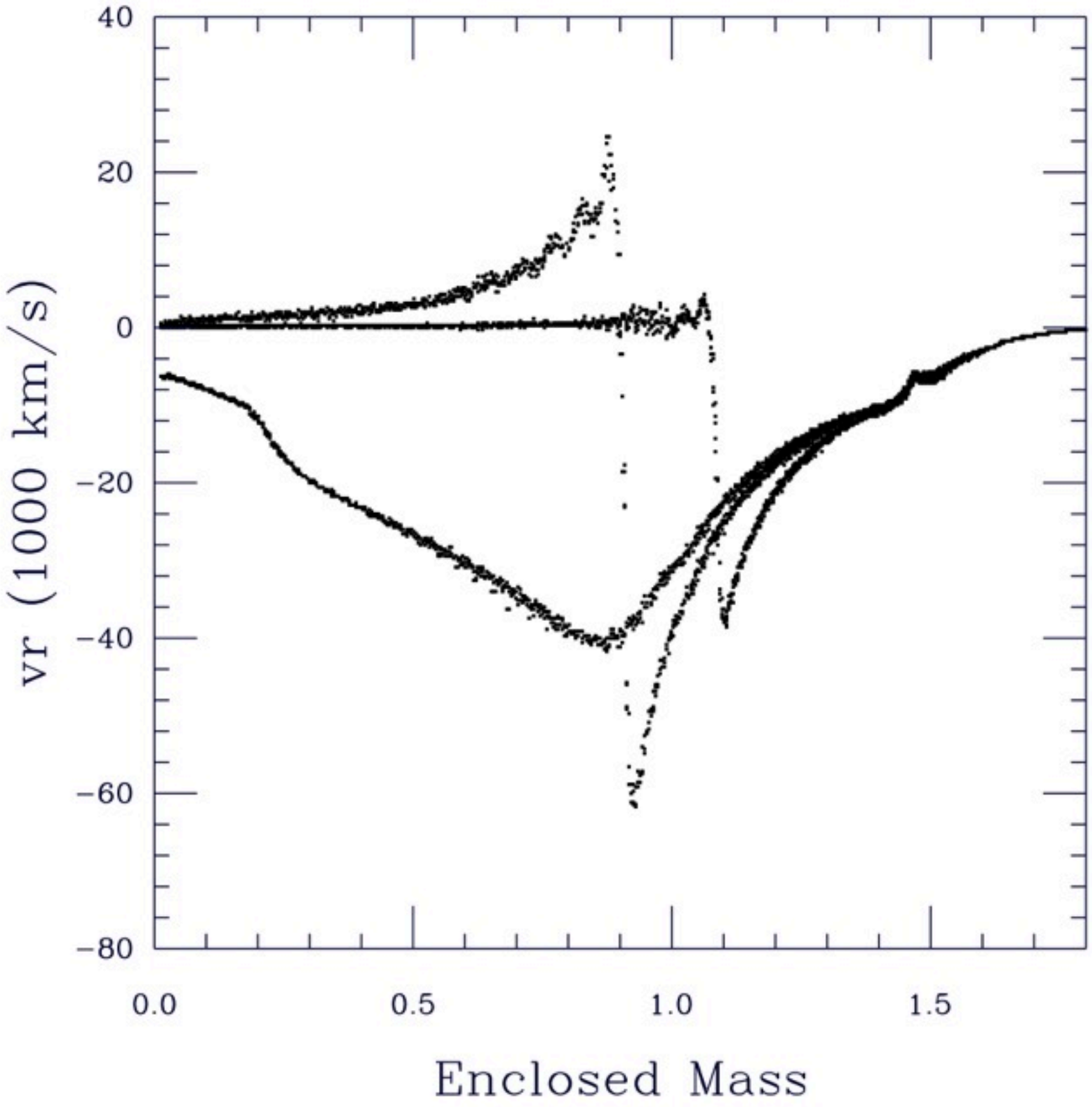

FIG. 22: Collapse and bounce of the iron core in a 13 $M_\odot$ supernova. Radial velocity vs. enclosed mass at -0.5 ms, +0.2 ms, and 2.0 ms with respect to bounce. The blip at 1.5 $M_\odot$ is due to the explosive nuclear burning of oxygen in the infall (Herant & Woosley, unpublished).

Woosley, Heager & Weaver 2002

Neutrinos

1. Nearly massless
2. Spin 1/2 (Lepton)
3. Produced in β Decay (proposed to explain energy loss during decay)
4. Interact only through the weak force, hence they can readily travel through matter at nearly the speed of light

Neutrinos detected from SN 1987a

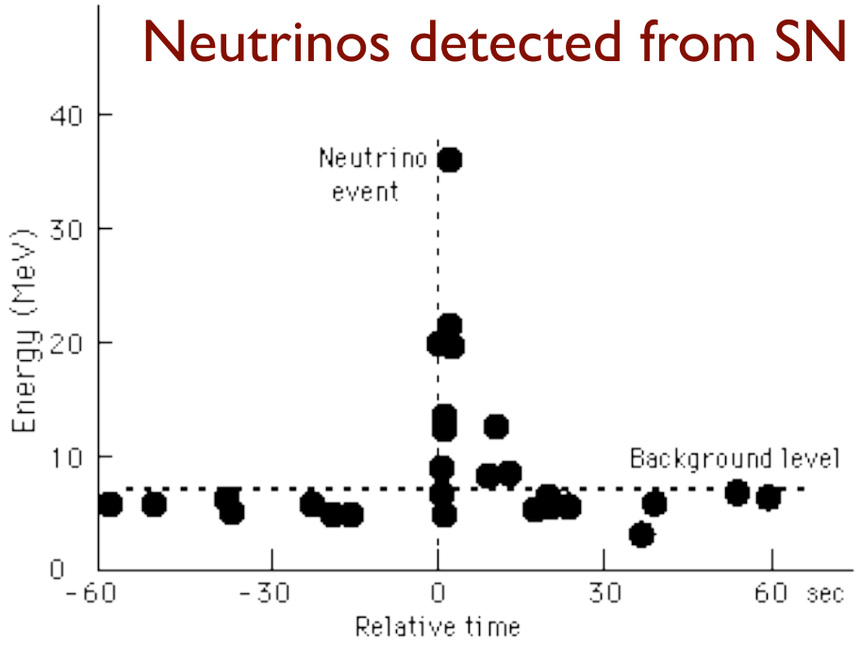

Neutrinos Losses and Heating

Neutrinos are produced during nuclear burning.

As temperatures approach a billion K, a population of thermalized positions and electon pairs are created. These can annihilate and sometimes produce neutrino/antineutrion pairs.

$e^+ + e^- \Rightarrow \gamma \Rightarrow \nu + \nu^*$

These can escape, leading to major source of energy. Also, during core collapse,

$p + e^- \Rightarrow n + \nu$

During core collapse, 10% of the rest mass is emitted in neutrinos, about 3×10^{53} ergs in a few seconds. This stops accretion and prevents the core from becoming a black hole.

About $1\text{-}2 \times 10^{51}$ ergs is then converted into kinetic energy through neutrino heating

Neutrinos Losses

TABLE 1 Evolution of a 15-solar-mass star.

Stage	Time Scale	Fuel or Product	Ash or product	Temperature (10^9 K)	Density (gm/cm^3)	Luminosity (solar units)	Neutrino Losses (solar units)
Hydrogen	11 My	H	He	0.035	5.8	28,000	1800
Helium	2.0 My	He	C,O	0.18	1390	44,000	1900
Carbon	2000 y	C	Ne,Mg	0.81	2.8×10^5	72,000	3.7×10^5
Neon	0.7 y	Ne	O,Mg	1.6	1.2×10^7	75,000	1.4×10^8
Oxygen	2.6 y	O,Mg	Si,S,Ar, Ca	1.9	8.8×10^6	75,000	9.1×10^8
Silicon	18 d	Si,S,Ar, Ca	Fe,Ni, Cr,Ti,...	3.3	4.8×10^7	75,000	1.3×10^{11}
Iron core collapse[a]	~1 s	Fe,Ni, Cr, Ti,...	Neutron Star	> 7.1	$>7.3 \times 10^9$	75,000	$>3.6 \times 10^{15}$

[a]The presupernova star is defined by the time when the contraction speed anywhere in the iron core reaches 1,000 km s^{-1}.

Woosley and Janka 2005

Neutrinos Heating

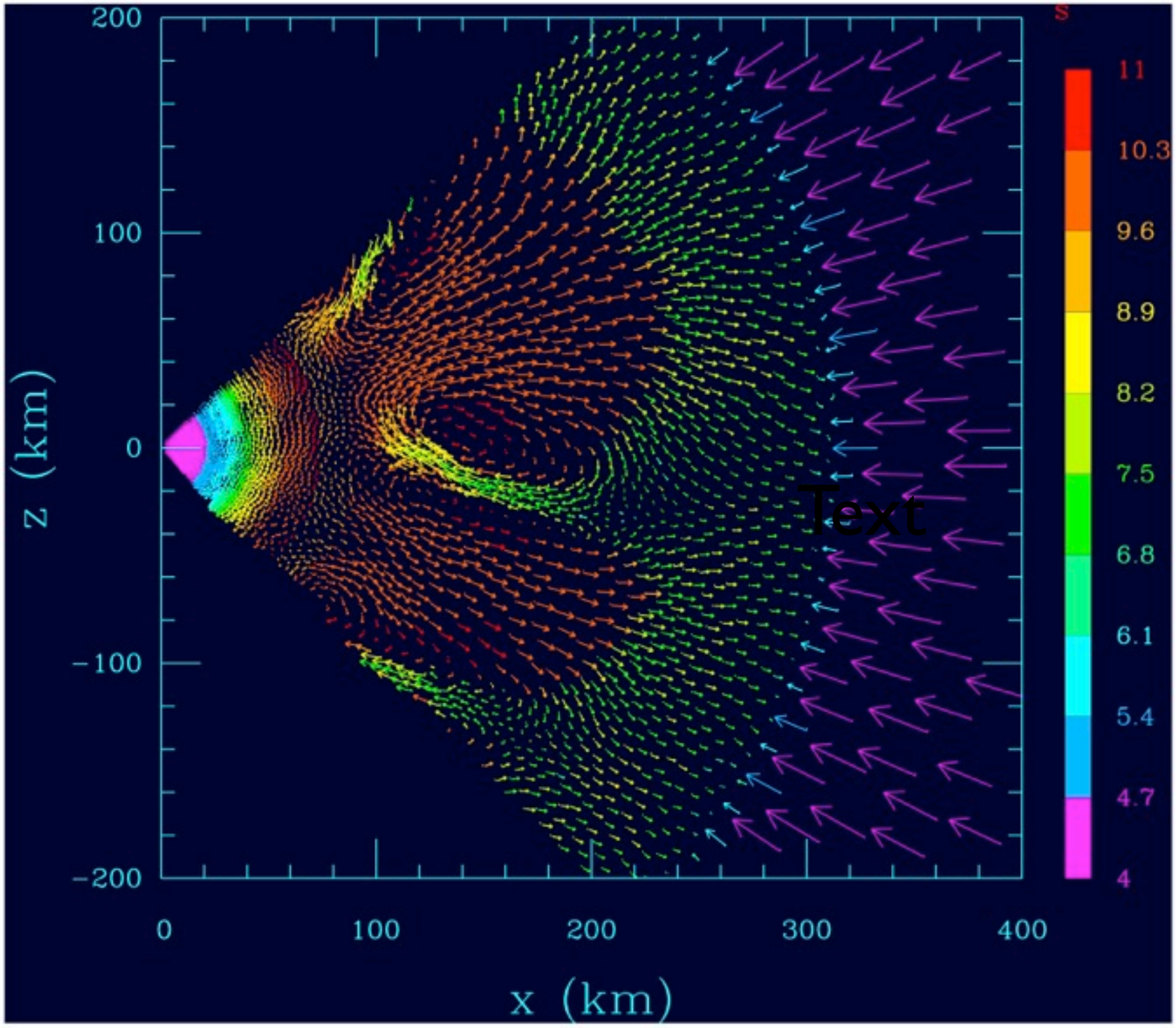

FIG. 23: Neutrino driven convection 50 ms after the bounce of the core of a 13 $M_\odot$ supernova. The entropy is color coded (Herant and Woosley, unpublished).

Neutrinos are absorbed by the reactions:

$$p + \nu \Rightarrow n + e^+$$

$$n + \nu \Rightarrow p + e^-$$

This inflaces bubble of photons and electron positron pairs which drives explosion.

This hot gas is convectively unstable.

Text

Woosley and Janka 2005

From Bounce to Explosion

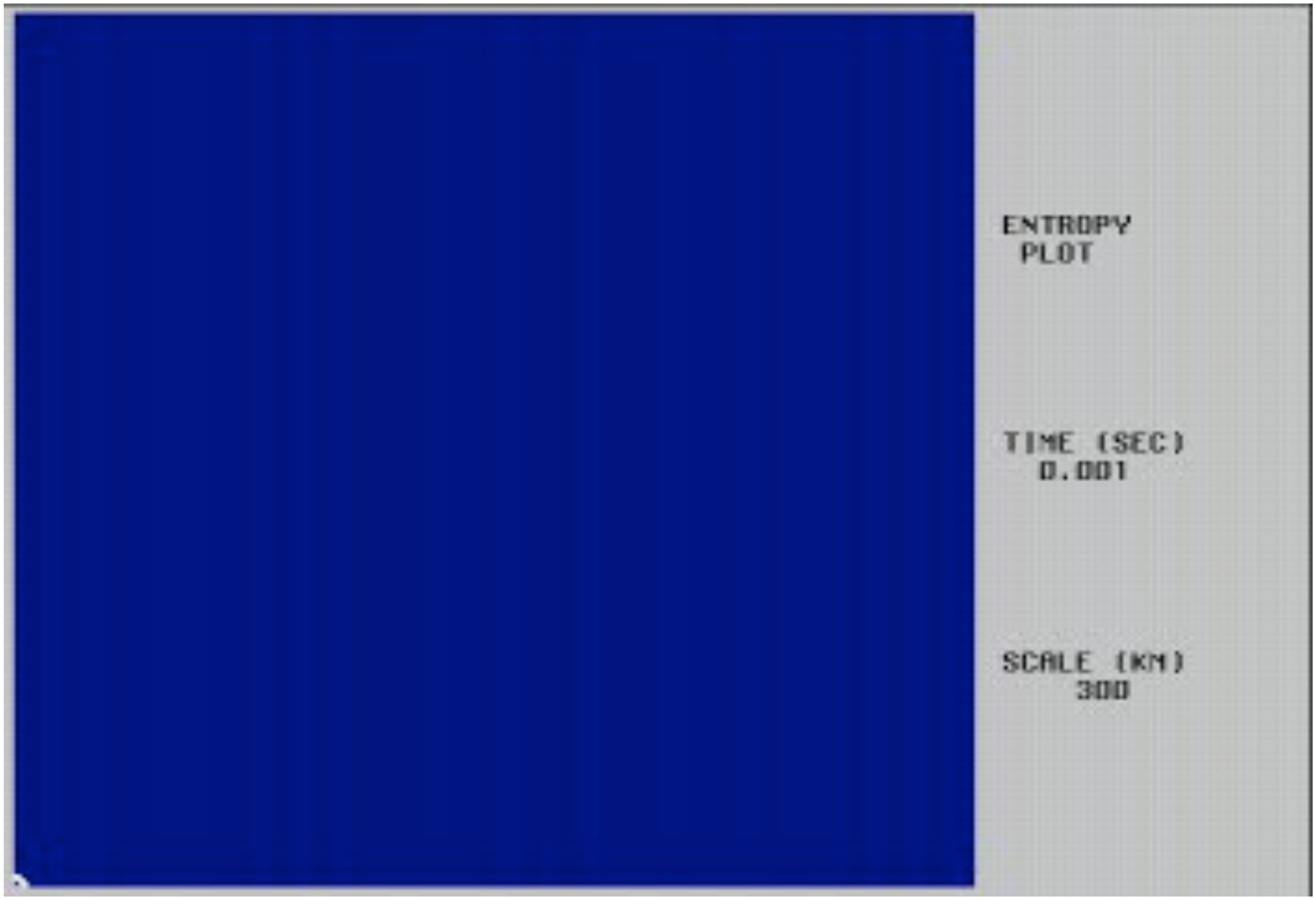

From Bounce to Explosion

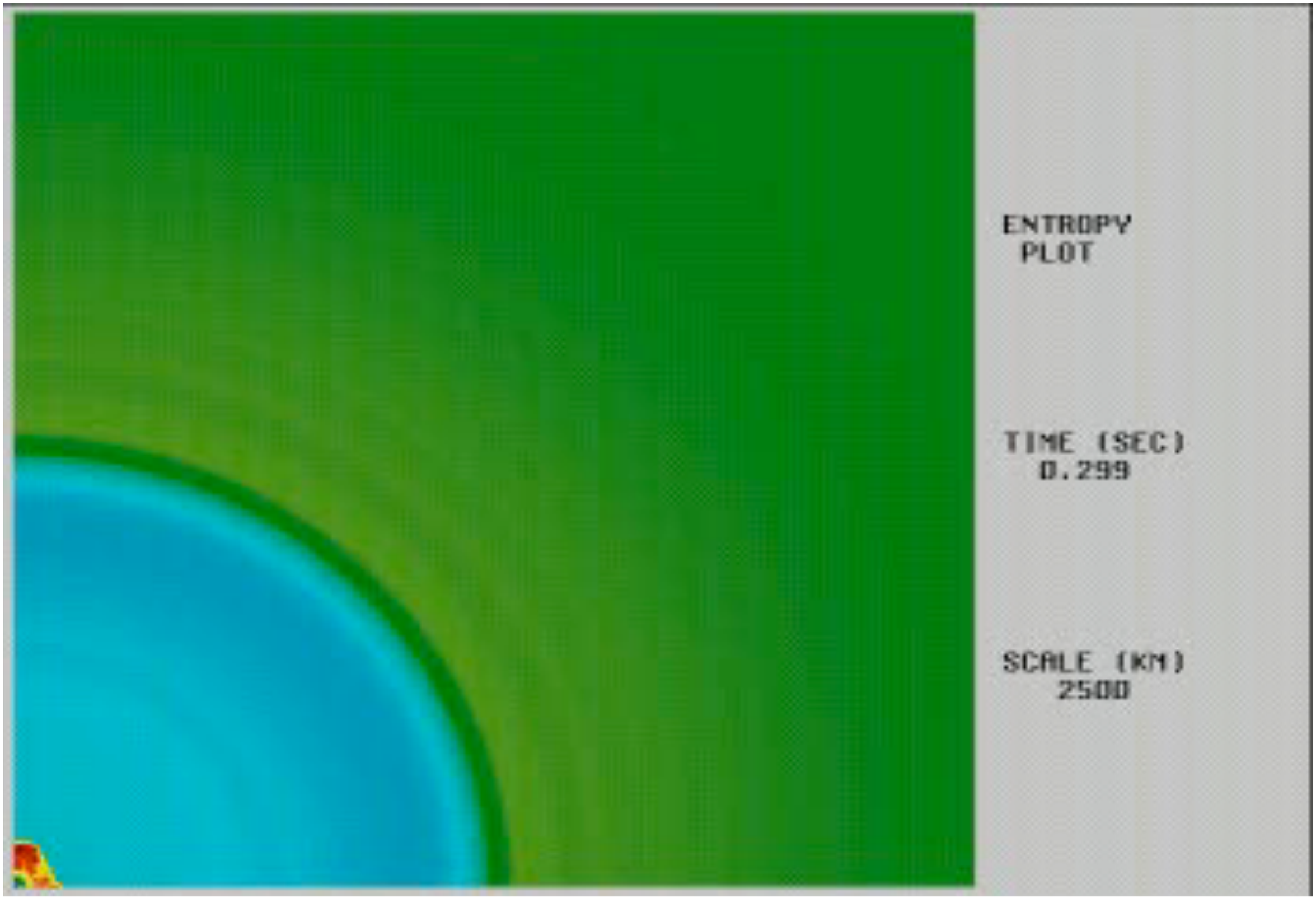

Burrows et al. 1995

The Explosion

Buoyant bubbles push outward, creating shock waves as they rise.

The snapshots are for sizes of of 200, 300, 500 and 2000 km s^{-1}

Note the turbulent, bubbling morphology.

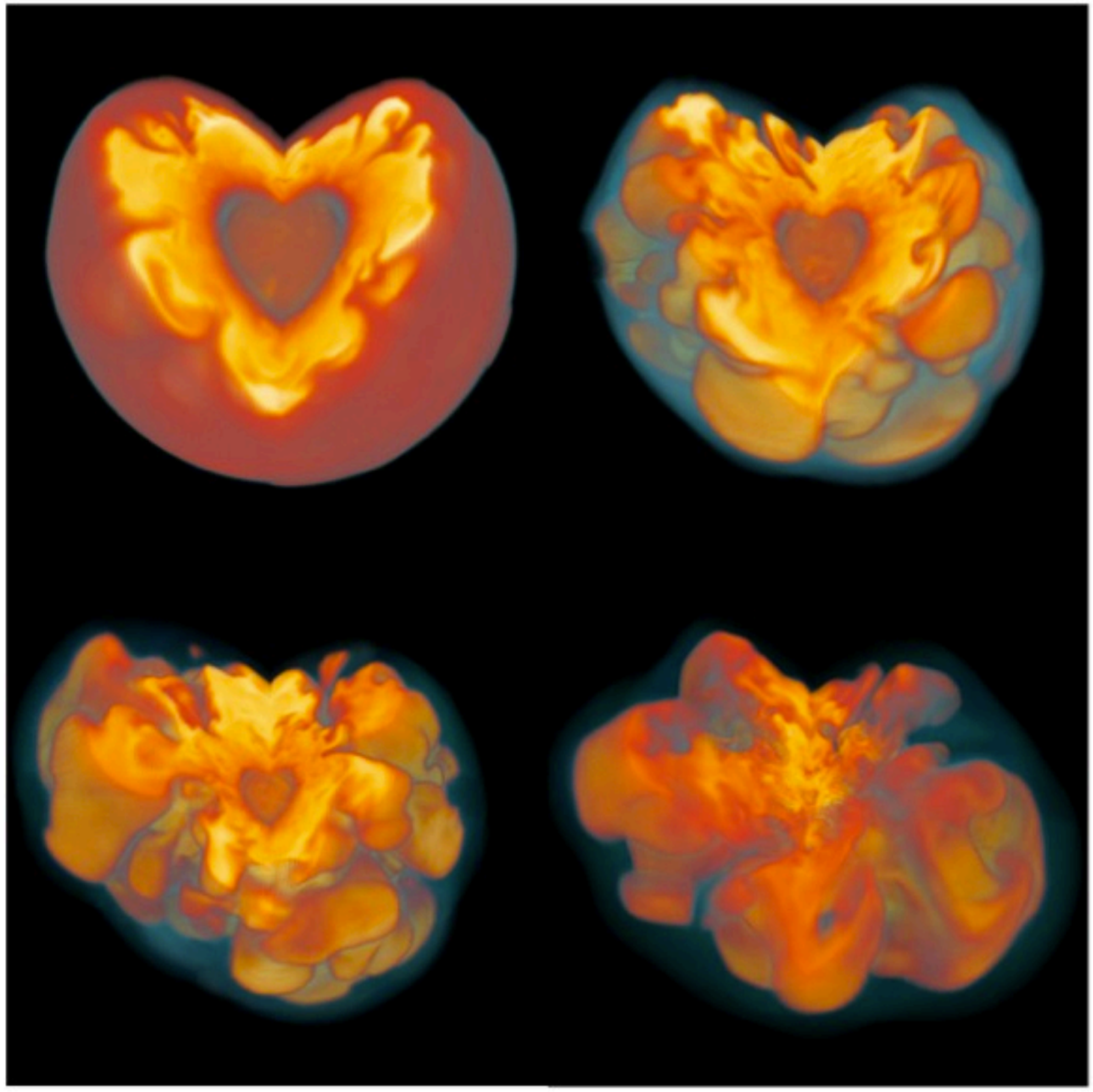

Figure 2: *Looking into the heart of a supernova (14). Four snapshots show the vigorous boiling of the neutrino-heated, convective region around the nascent neutron star. Buoyant bubbles of hot matter moving outwards appear bright red and yellow. These are bounded by a shock wave, which expands outwards, disrupting the star. The images, from top left to bottom right, show the structure at 0.1, 0.2, 0.3, and 0.5 seconds after the shock is born. At these times, the shock has an average radius of about 200, 300, 500, and 2,000 kilometers, respectively.*

Woosley and Janka 2005

The Explosion

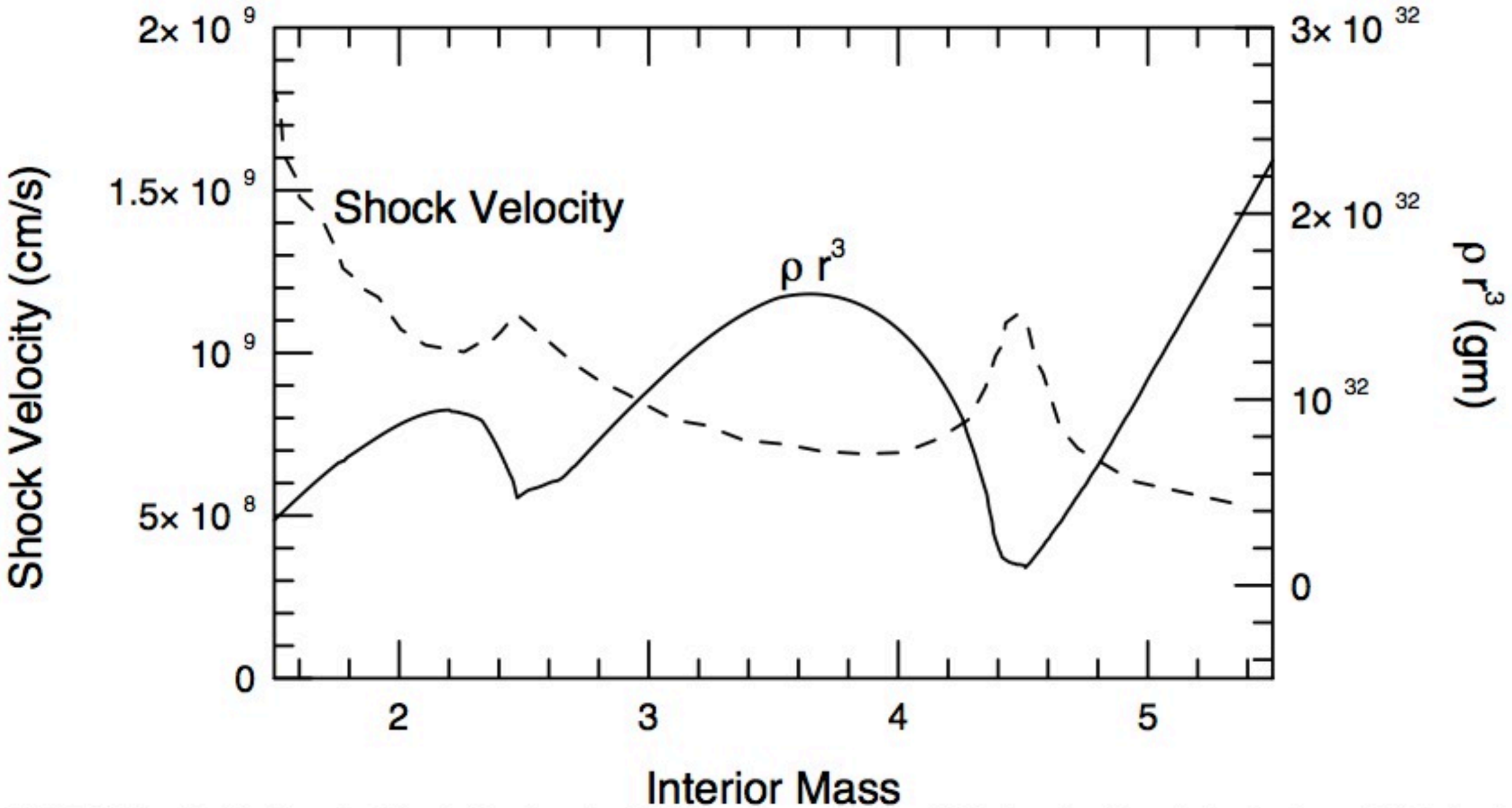

FIG. 24: The distribution of ρr^3 in the interior of a 15 $M_\odot$ presupernova star (right-hand axis) and the shock speed (left-hand axis) as a function of mass for an explosion of 1.2×10^{51} erg. The 15 $M_\odot$ progenitor is a red supergiant. Note that the correlation between shock acceleration and declining ρr^3. When the shock decelerates it leaves behind a region that is unstable to mixing. The edge of the helium core is at 4.2 $M_\odot$ so a large degree of mixing occurs as the helium core runs into the hydrogen envelope. Figure from Woosley & Weaver (1995).

Woosley, Heager & Weaver 2002

The Explosion

Turbulences mixes elements from different layers

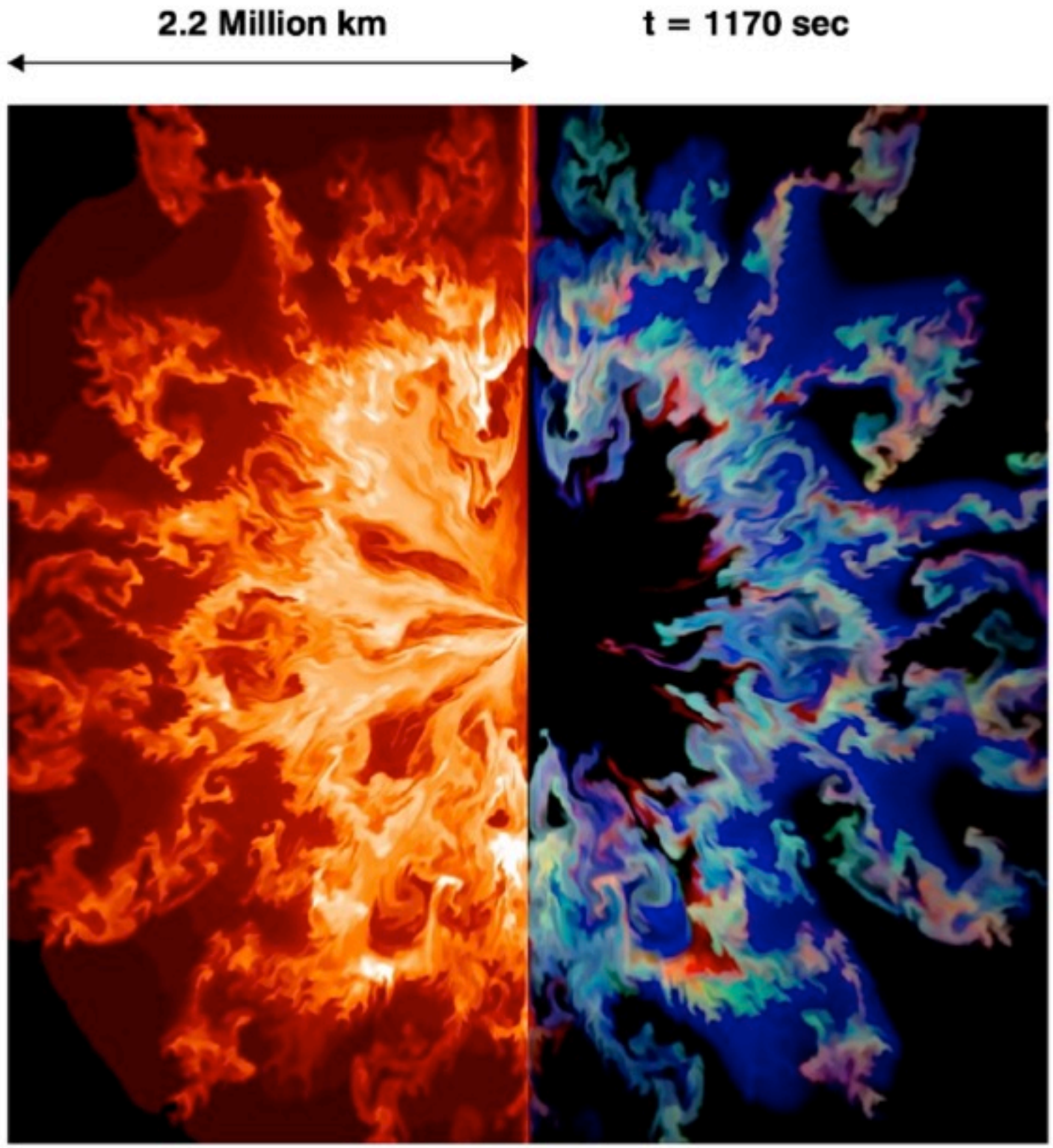

FIG. 25: Mixing in the explosion of a 15 $M_\odot$ red supergiant (Kifonidis et al. 2000).

Woosley and Janka 2005

The Explosion

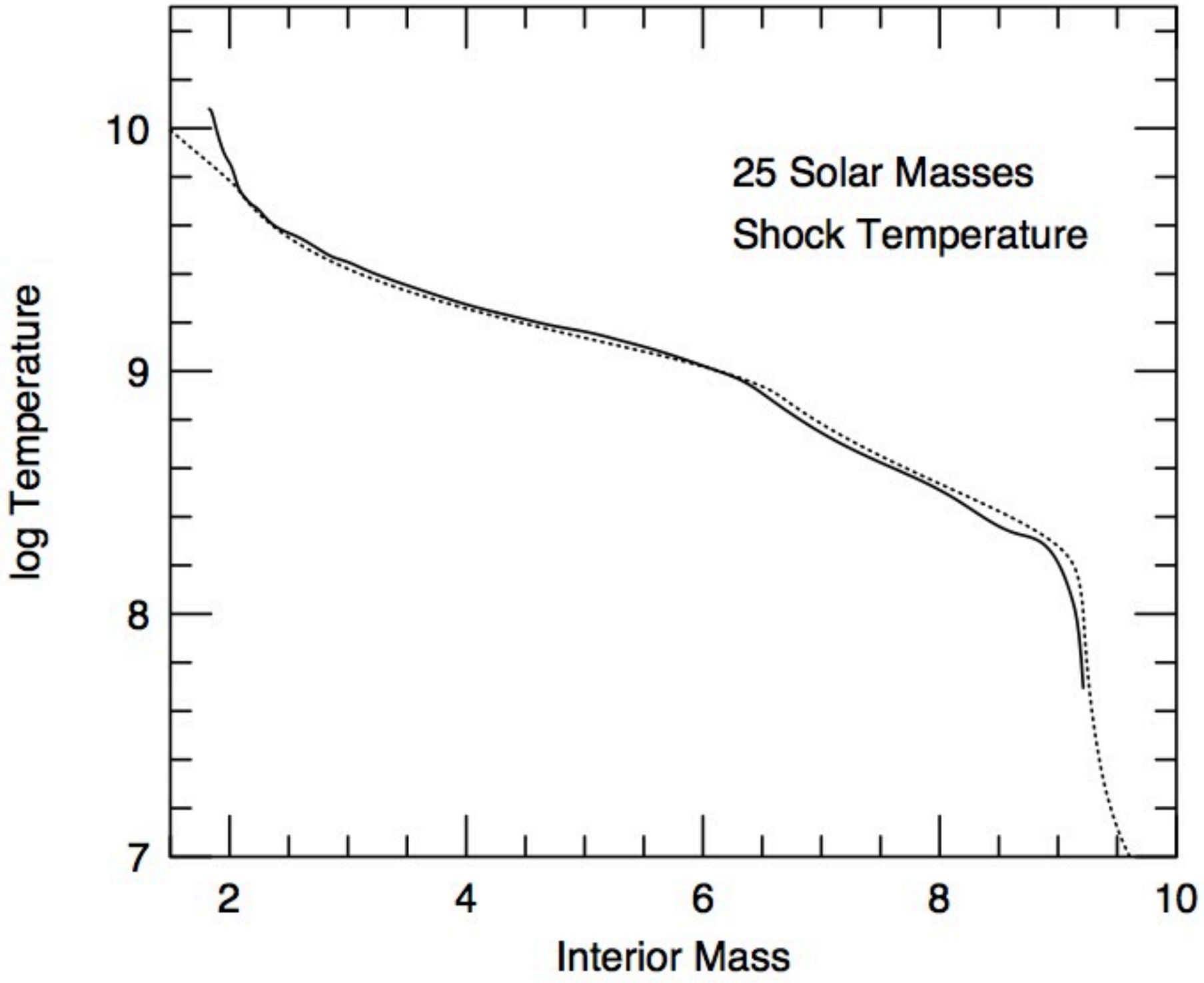

FIG. 26: Shock temperature as a function of mass for a 25 $M_\odot$ supernova of final kinetic energy at infinity of 1.2×10^{51} erg. The dashed line is an approximation, eq. (37), discussed in the text.

Woosley, Heager & Weaver 2002

The Jet

Neutrons stars can have velocities of 300-400 kms^{-1}, sometimes as high as 1000 km s^{-1}.
This may be driven by asymmetries in the inner motions due to convection.

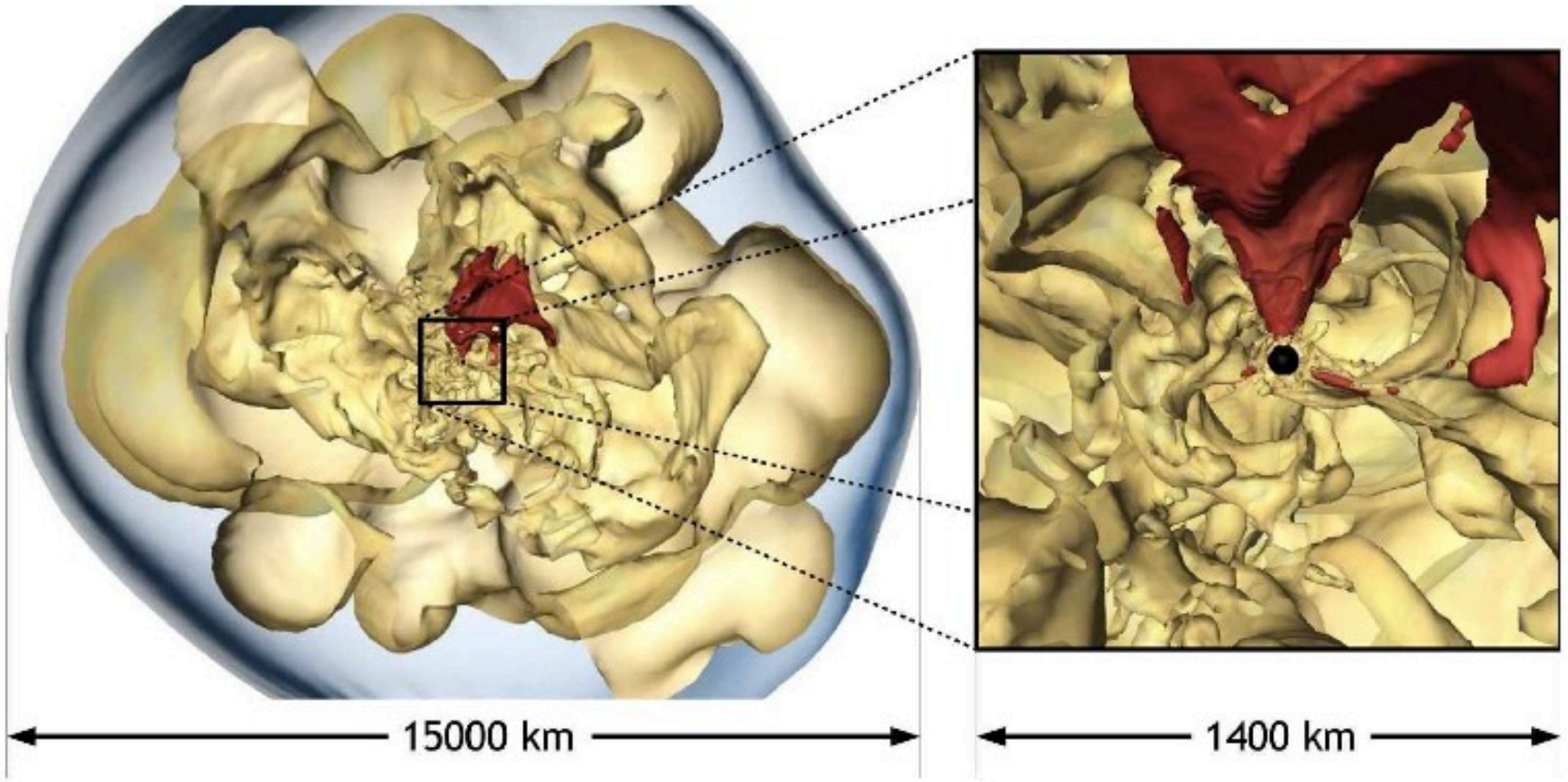

Figure 3: *Accretion onto the nascent neutron star shows a dipolar character (15). Cool matter (visible in red in the blow-up on the right) falls and is funnelled onto one side of the neutron star (black circle at the center), while neutrino-heated, hot ejecta flows out on the other. This 'jet engine' can accelerate the neutron star to velocities of several hundred kilometres per second within the first second of its life. At that same time, the supernova shock wave (blue, enveloping surface) is already well on its way through the exploding star (left panel), being pushed by the buoyant bubbles of neutrino-heated gas. Although the calculation was followed in three spatial dimensions, the initial model was spherically symmetric and was not rotating.*

Woosley and Janka 2005

The Neutrino Driven Neutron Wind

Antineutrinos captured by protons create neutron wind for about 10 seconds

As expanding gas coolse, these particles combine with protons to creates alpha particle

Further cooling results in seed nuclei

Then wind then drives the r-process

Woosley and Janka 2005

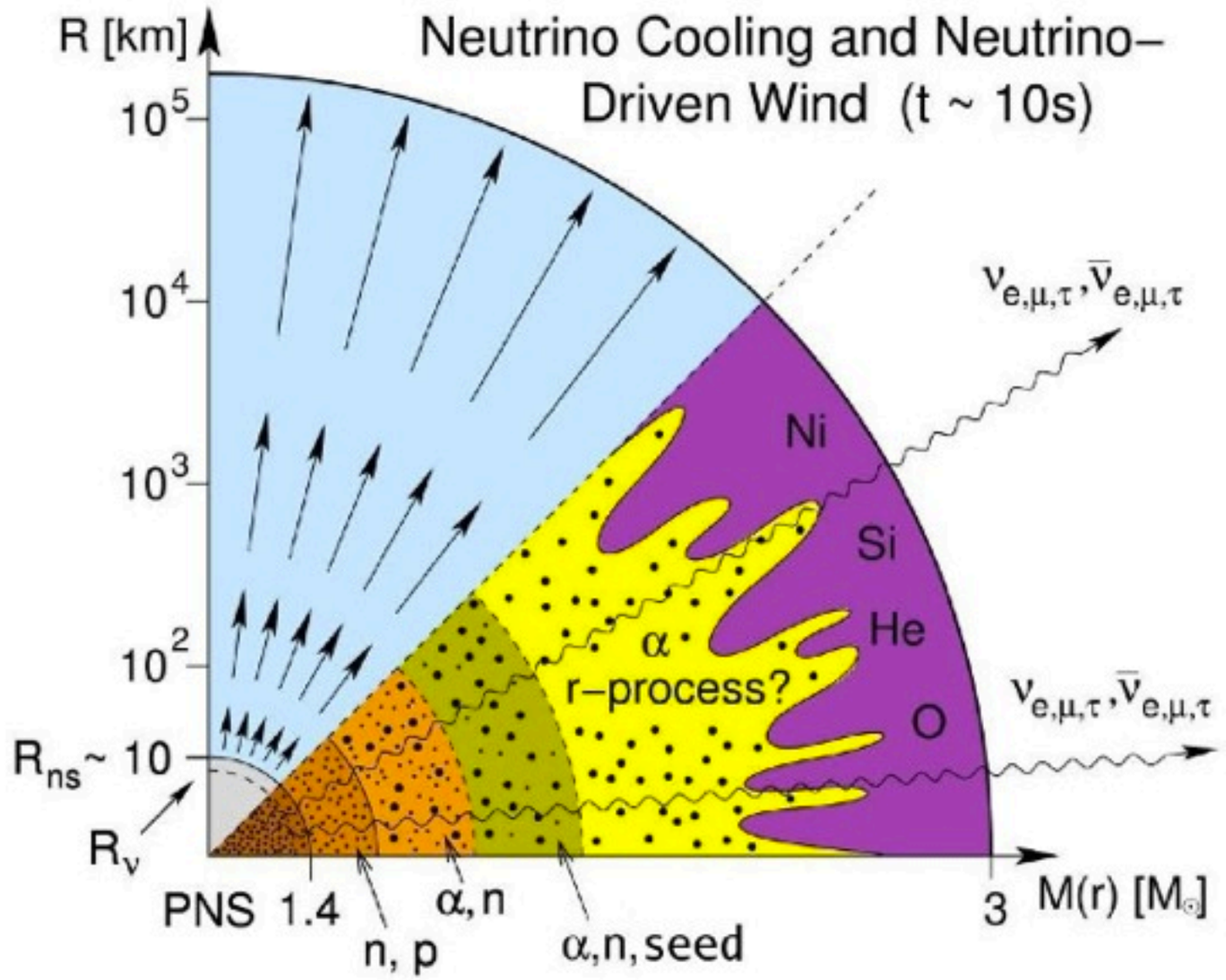

Figure 5: *Neutrinos (ν_e,ν_μ,ν_τ and their anti-particles) drive a wind from the surface of the cooling proto-neutron star (PNS) creating the r-process isotopes. The wind begins as a flux of neutrons and protons lifted from the surface of the PNS (here 1.4 solar masses and 10 km in radius) by neutrinos originating at the "neutrinosphere" (R_ν). As these nucleons flow out, an excess of neutrons is created by the capture of anti-neutrinos on protons. As the nucleons cool, all the available protons combine with neutrons to make α-particles until one is left, in the orange region, with a mixture of only α-particles and unbound neutrons. Further cooling leads to the assembly of a few α-particles into nuclei in the iron group ("seed") by reactions involving neutrons and α-particles (green region). As the temperature declines still further, from 3 billion K to 1 billion K, all neutrons are captured on this seed making the heavy r-process nuclei. Since the efficiency of the reactions that assemble α-particles into seed increases with the density, lower density in the wind keeps the number of seed small and makes the number of neutrons that can be captured on each larger.*

What Kind of Remnant?

Also - pair instability SN may have no remnant.

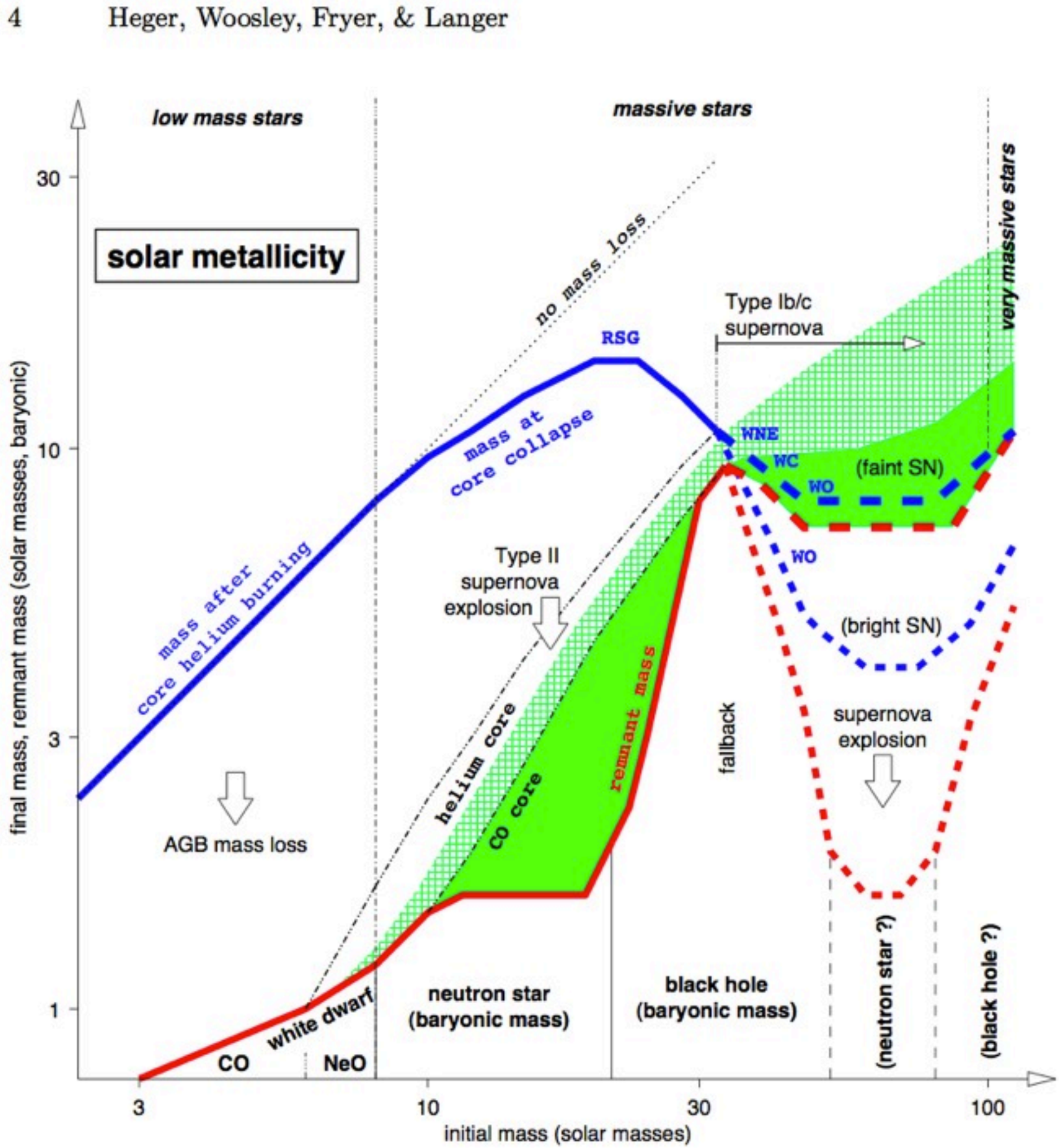

Woosley, Heager & Weaver 2002

Observations: Types of Supernova

Type I: No Hydrogen lines

Type Ia: Lack Hydrogen and Si II near light peak
Due to Collapse and detonation of white dwarf after it exceeds Chandrasekhar limit (by accreting gas or merger)

Type Ib: Non-ionized He and no SiII
Probably due to the core collapse of massive star.

Type Ic: Weak He and no SiII
Probably due to the core collapse of massive star.

Type II: Hydrogen lines - core collapse of massive star.

From an evolutionary perspective, the absence of RSGs at high luminosity and presence of H-rich WN stars in young massive clusters suggests the following variation of the Conti scenario in the Milky Way, i.e., for stars initially more massive than $\sim 75\ M_{\odot}$:

$$O \rightarrow \mathrm{WN(H-rich)} \rightarrow \mathrm{LBV} \rightarrow \mathrm{WN(H-poor)} \rightarrow \mathrm{WC} \rightarrow \mathrm{SN\,Ic},$$

whereas for stars of initial mass from ~ 40–$75\ M_{\odot}$,

$$O \rightarrow \mathrm{LBV} \rightarrow \mathrm{WN(H-poor)} \rightarrow \mathrm{WC} \rightarrow \mathrm{SN\,Ic},$$

and for stars of initial mass in the range 25–$40\ M_{\odot}$,

$$O \rightarrow \mathrm{LBV/RSG} \rightarrow \mathrm{WN(H-poor)} \rightarrow \mathrm{SN\,Ib}.$$

Crowther et al. 2007

Types of Supernova

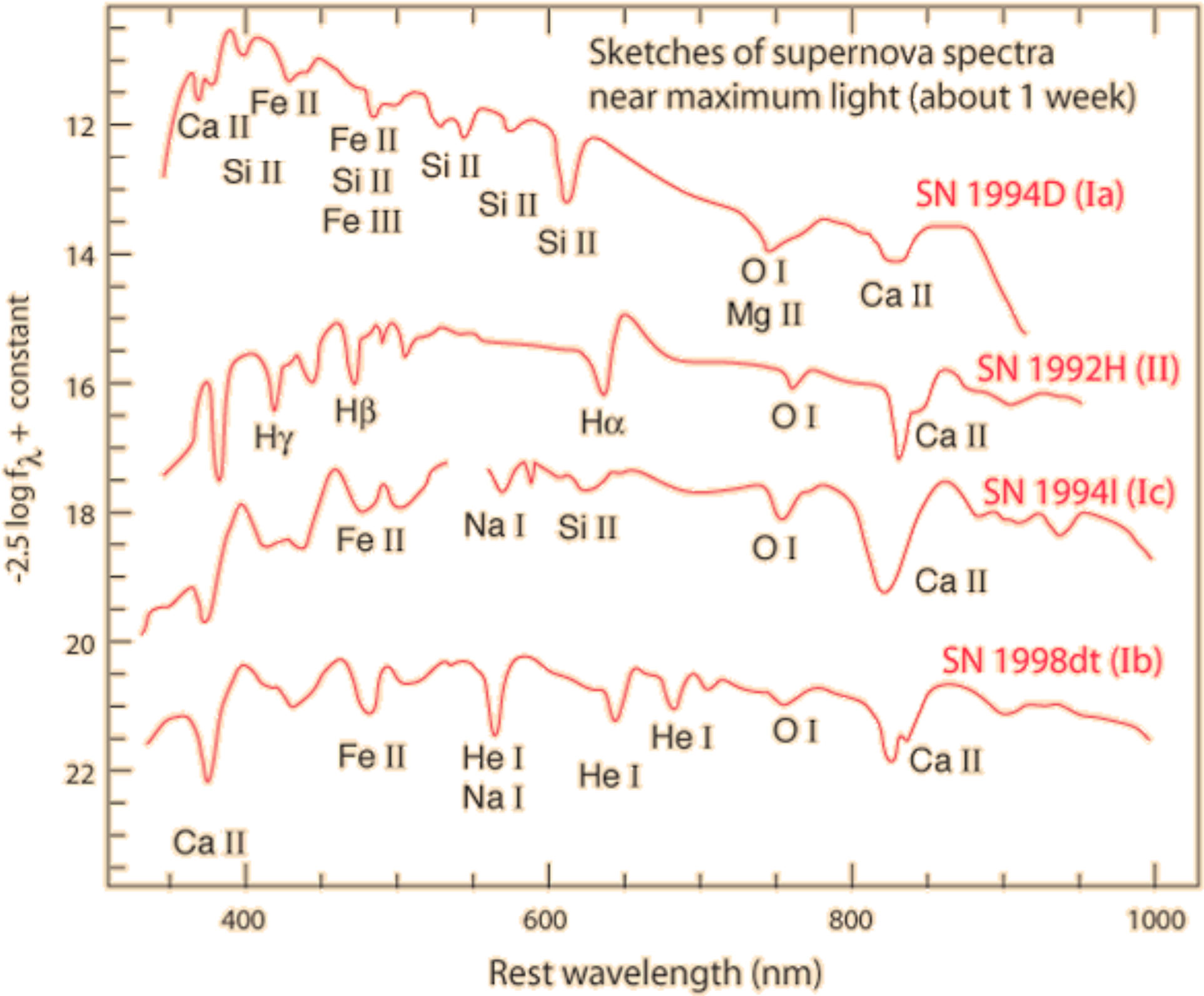

Sketches of spectra from Carroll & Ostlie, data attributed to Thomas Matheson of National Optical Astronomy Observatory.

Light Curves of Core Collapse Supernova

Tail of light curve powered by radioactive decay.

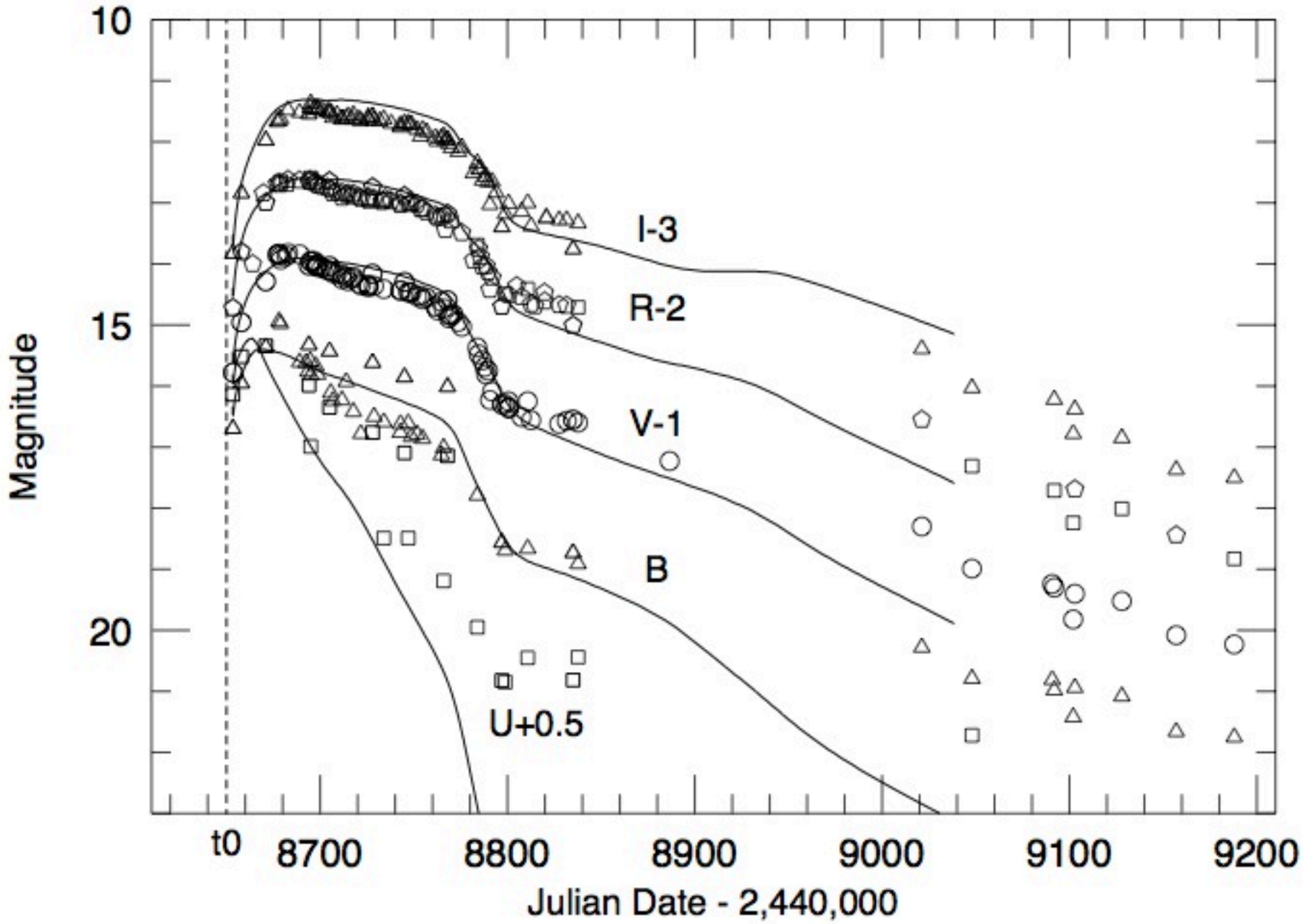

FIG. 30: Five color photometry of a model 15 $M_\odot$ supernova compared to observations of Type II-p SN 1992H (Eastman, Woosley, & Weaver 1994; Eastman et al. 1993, 1994). The I, R, V, and U magnitudes have been adjusted by the indicated shifts for plotting. The model calculations assume thermal level populations and the non-LTE corrections are appreciable particularly for the U-band. The supernova produced 0.06 $M_\odot$ of ^{56}Ni and the assumed distance modulus is 32.0, with no correction for extinction. Data are from Filippenko (1997).

Woosley, Heager & Weaver 2002

Supernova 1987a

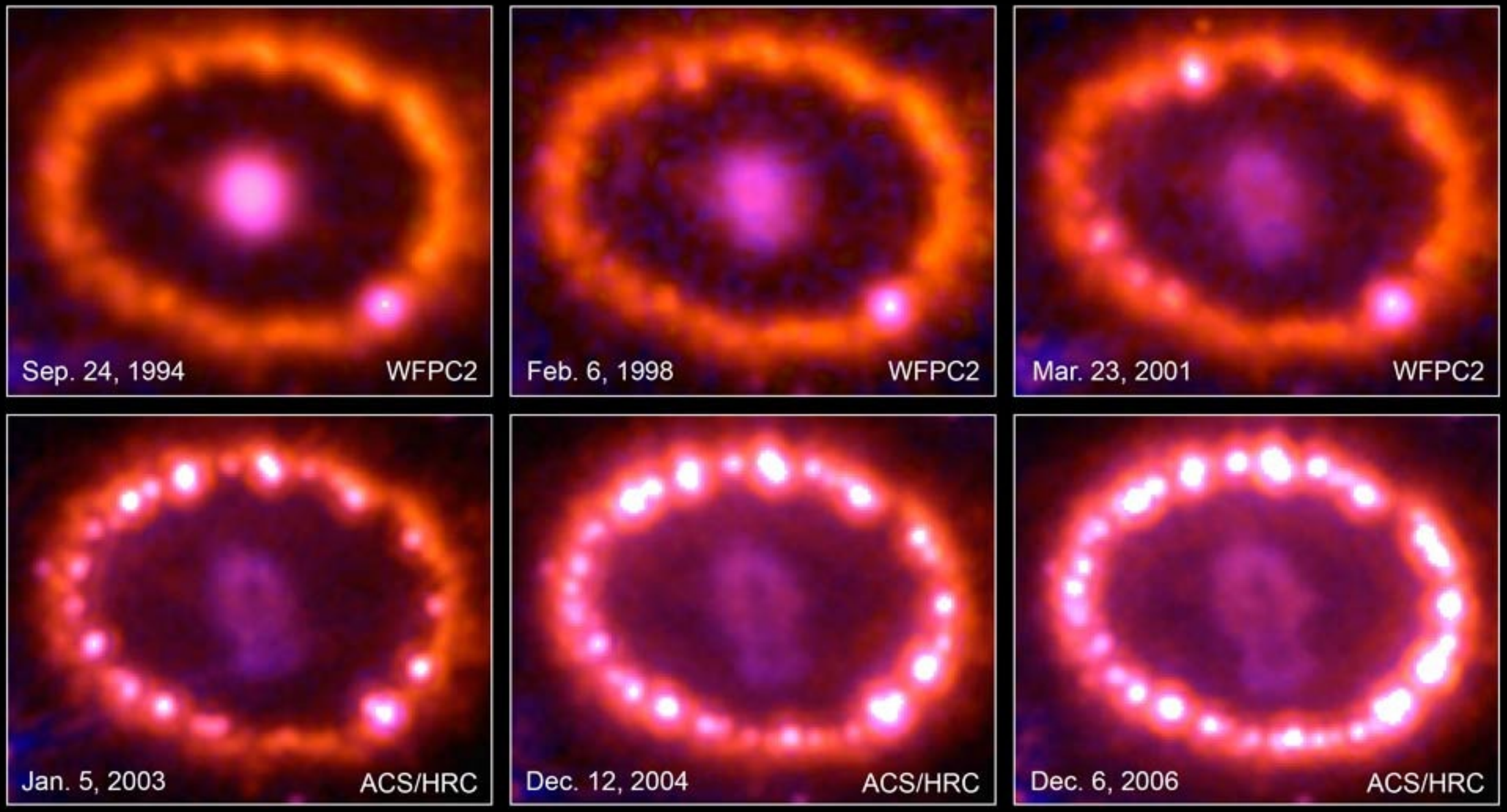

Supernova 1987A • 1994-2006

Hubble Space Telescope • WFPC2 • ACS

NASA, ESA, P. Challis, and R. Kirshner (Harvard-Smithsonian Center for Astrophysics)

STScI-PRC07-10b

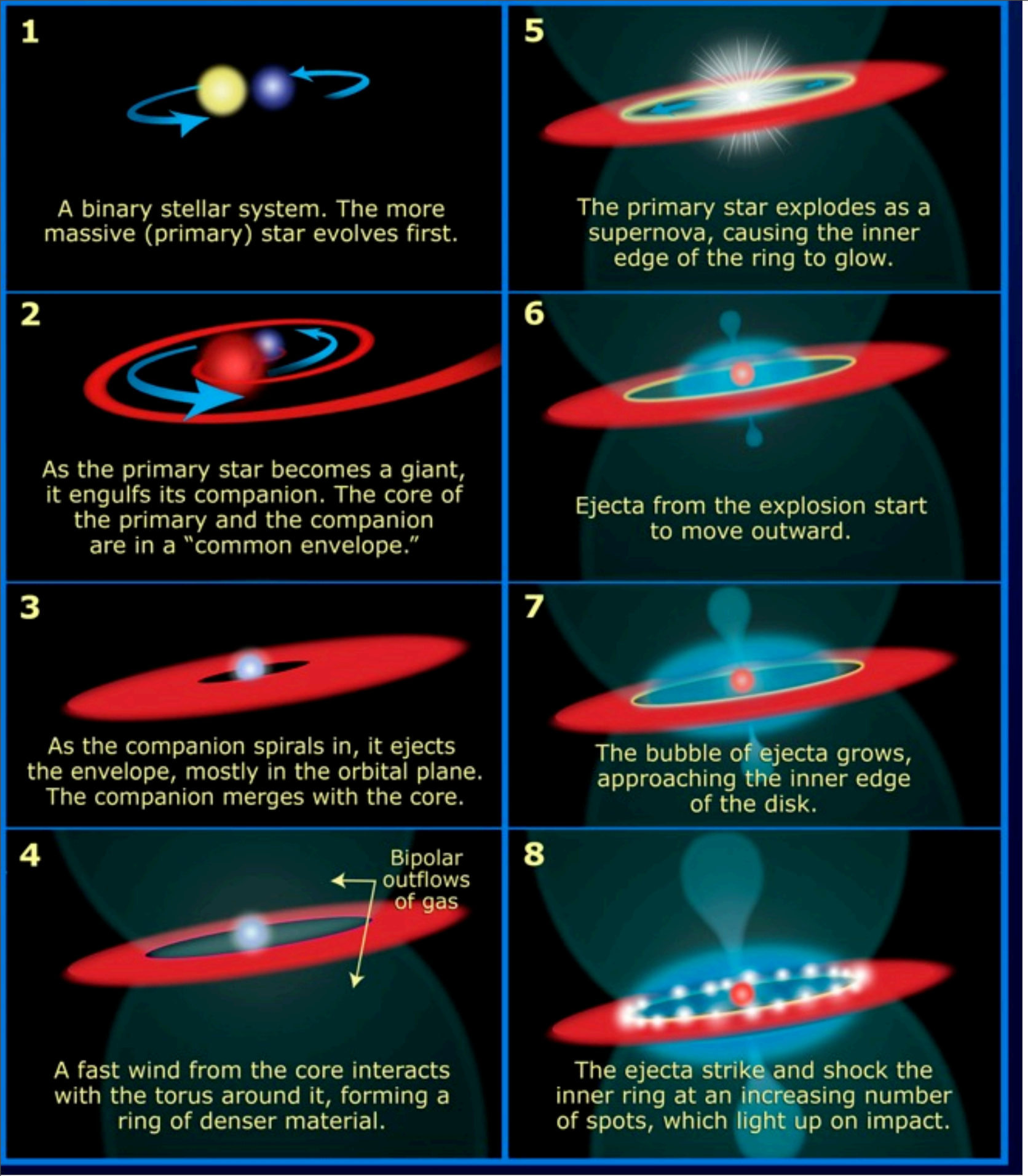

A Scenario for the necklace around SN 1987a

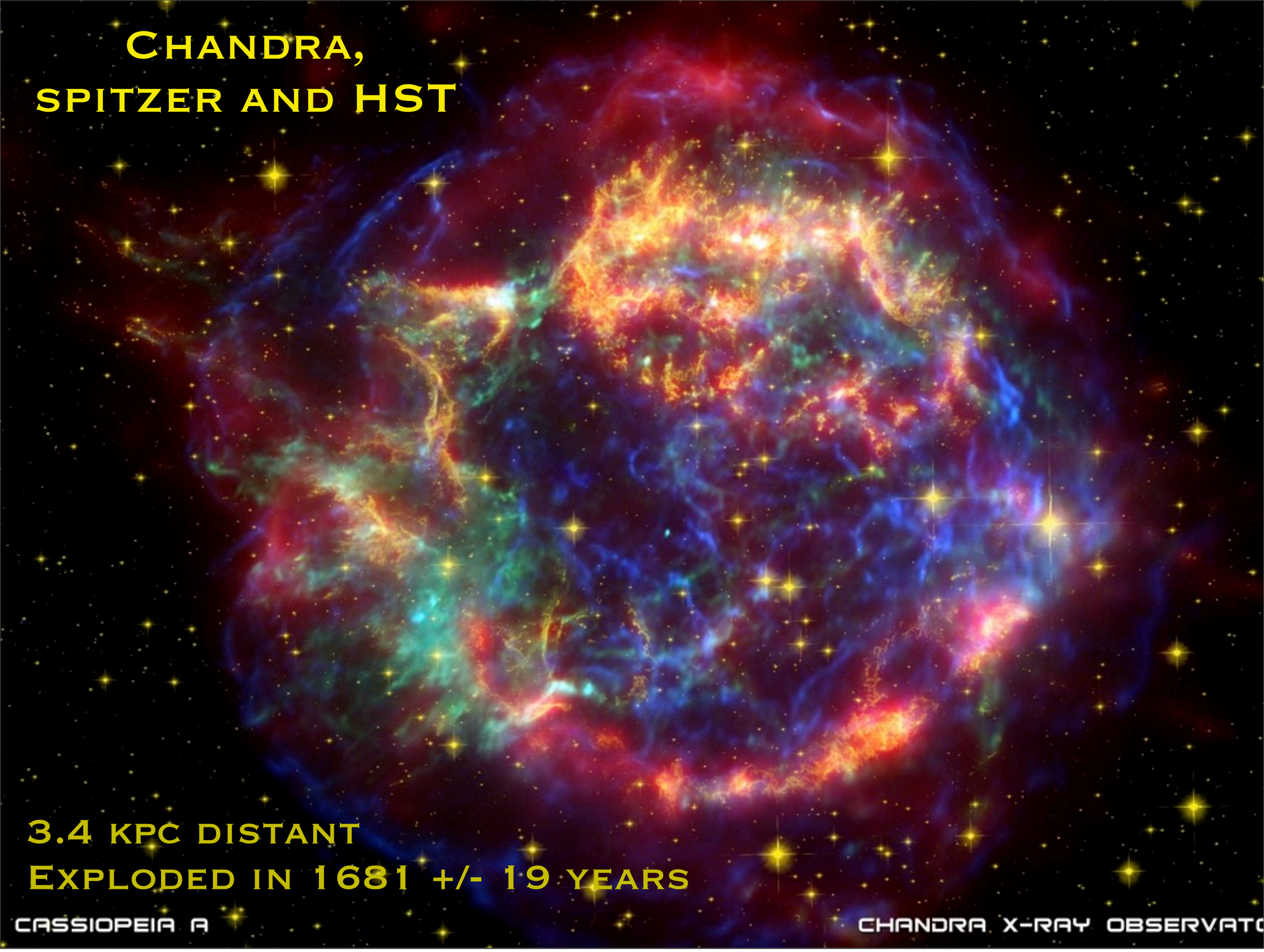
Chandra,
spitzer and HST
3.4 kpc distant
Exploded in 1681 +/- 19 years
CASSIOPEIA A
CHANDRA X-RAY OBSERVATO

Light Echoes

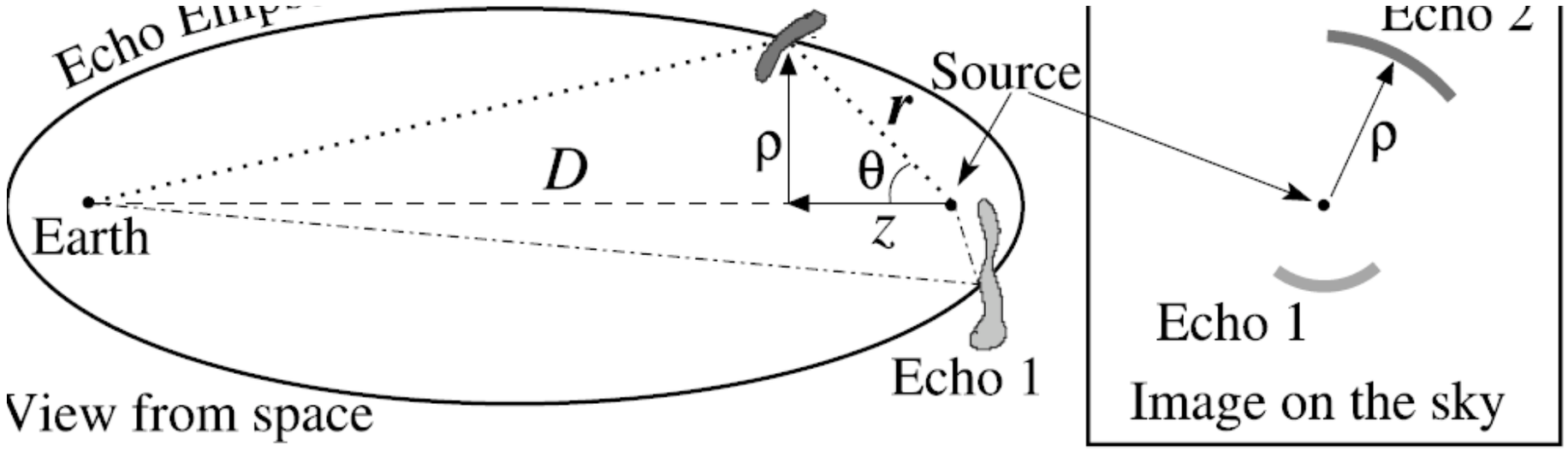

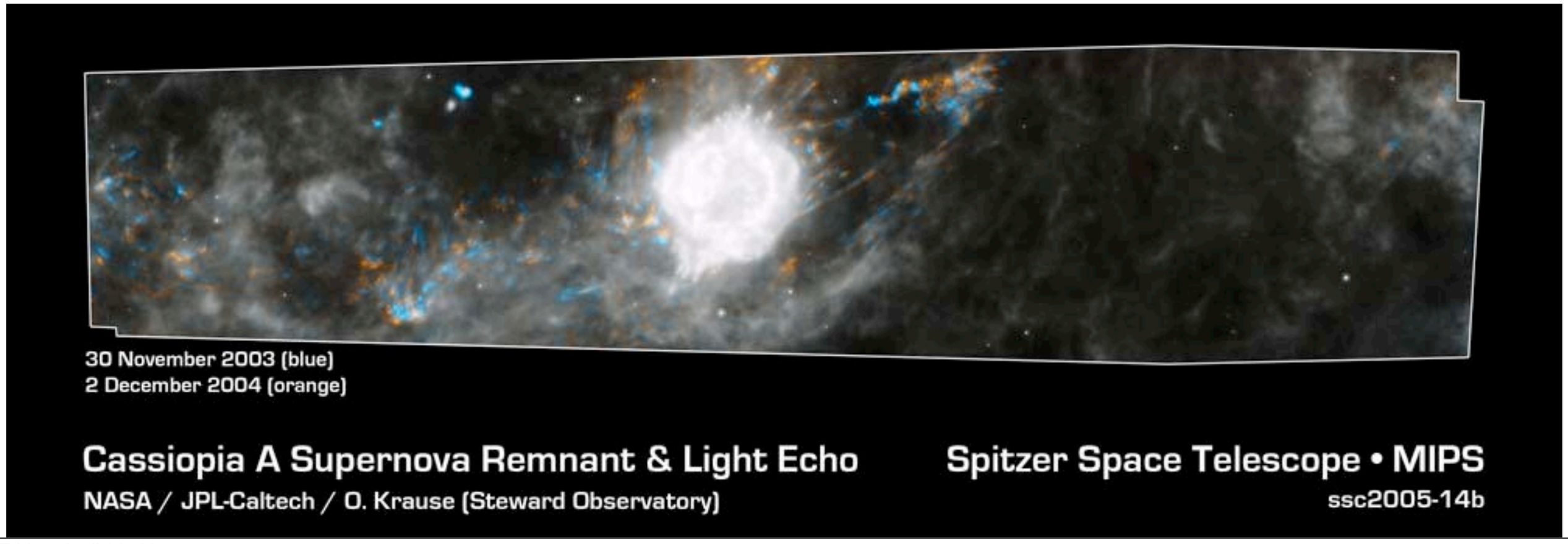

Light Echoes

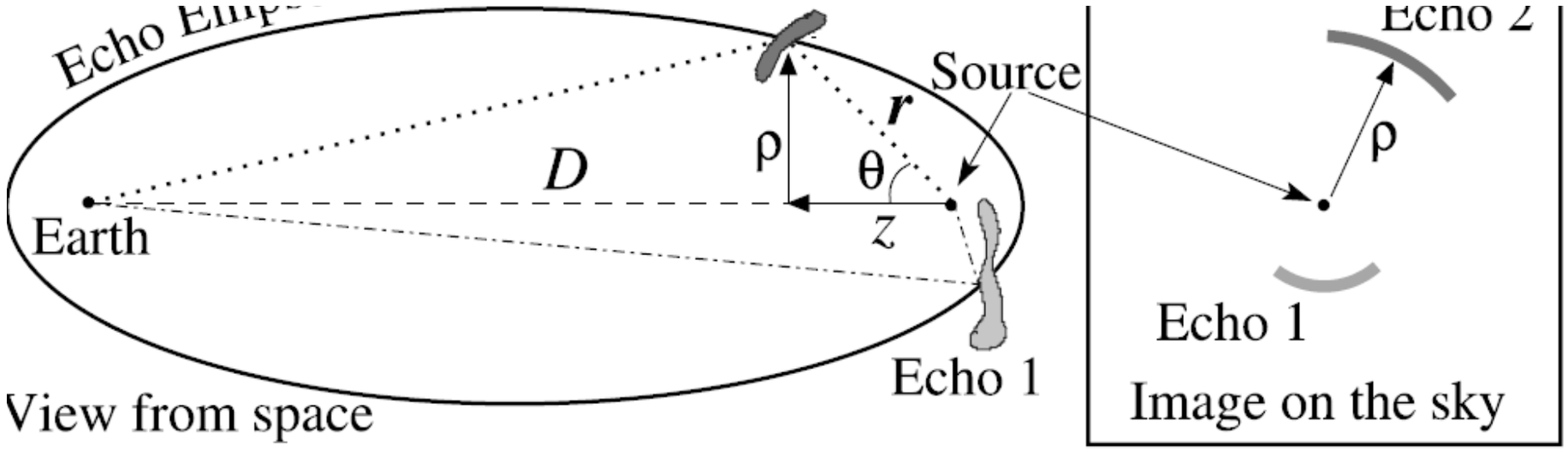

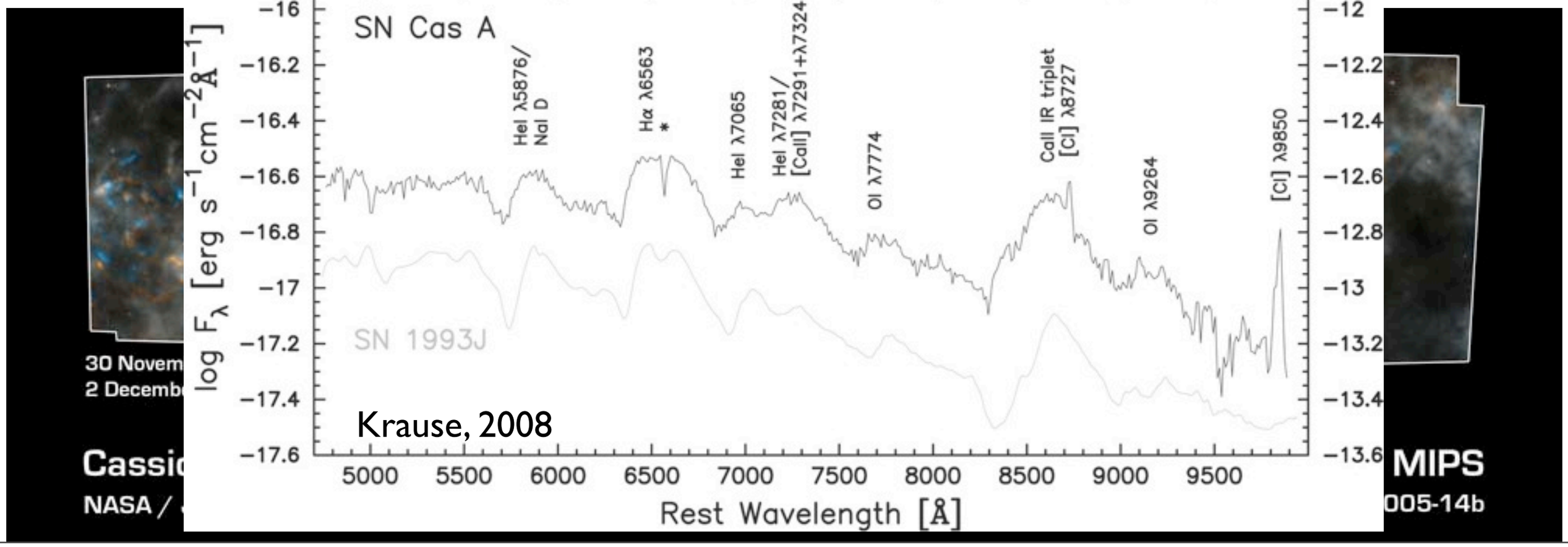

Cassiopeia A in multiple lines. First detection of "unshocked" ejecta as well as many elements in shocked gas.

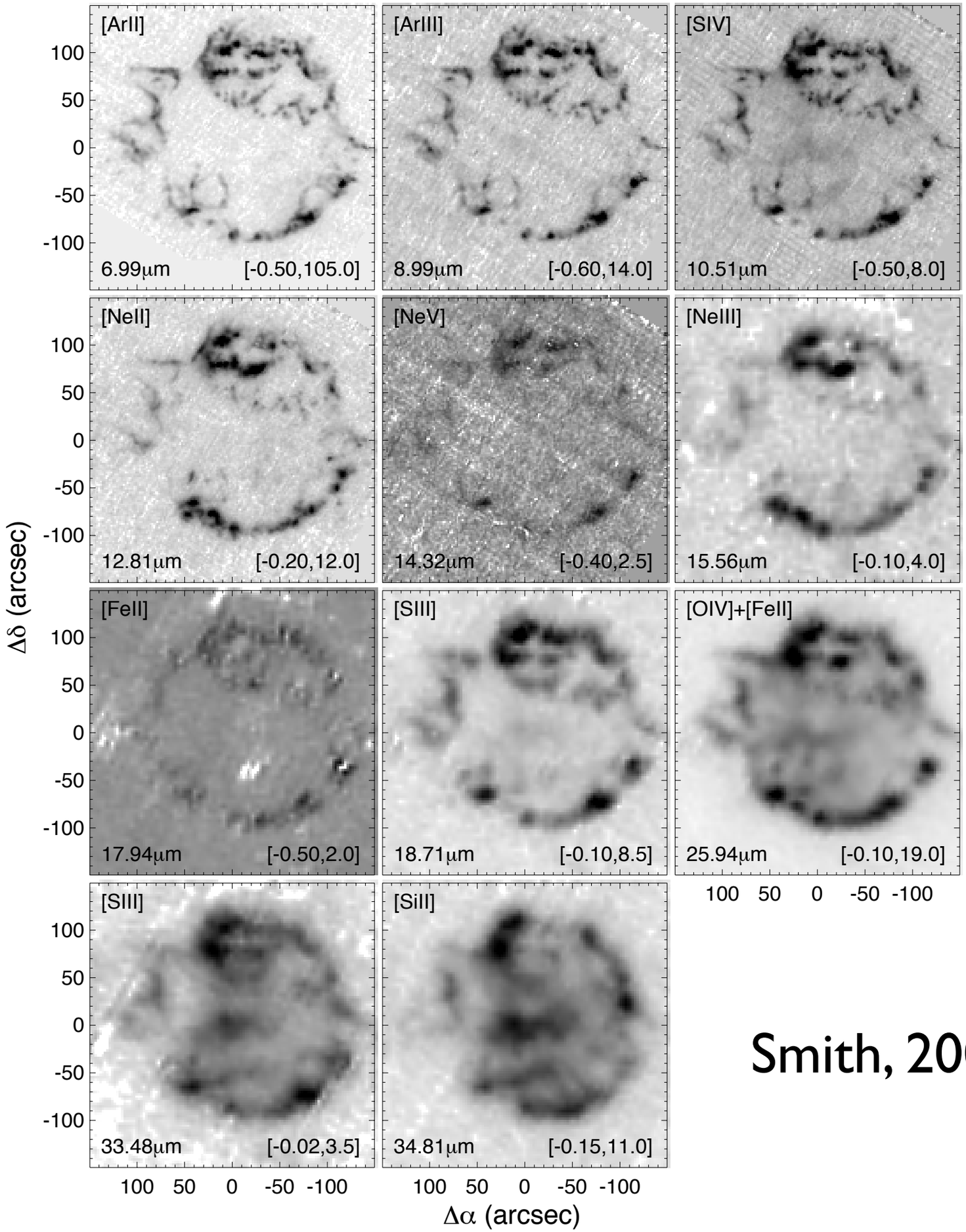

Smith, 2009

Cas A In 3D!

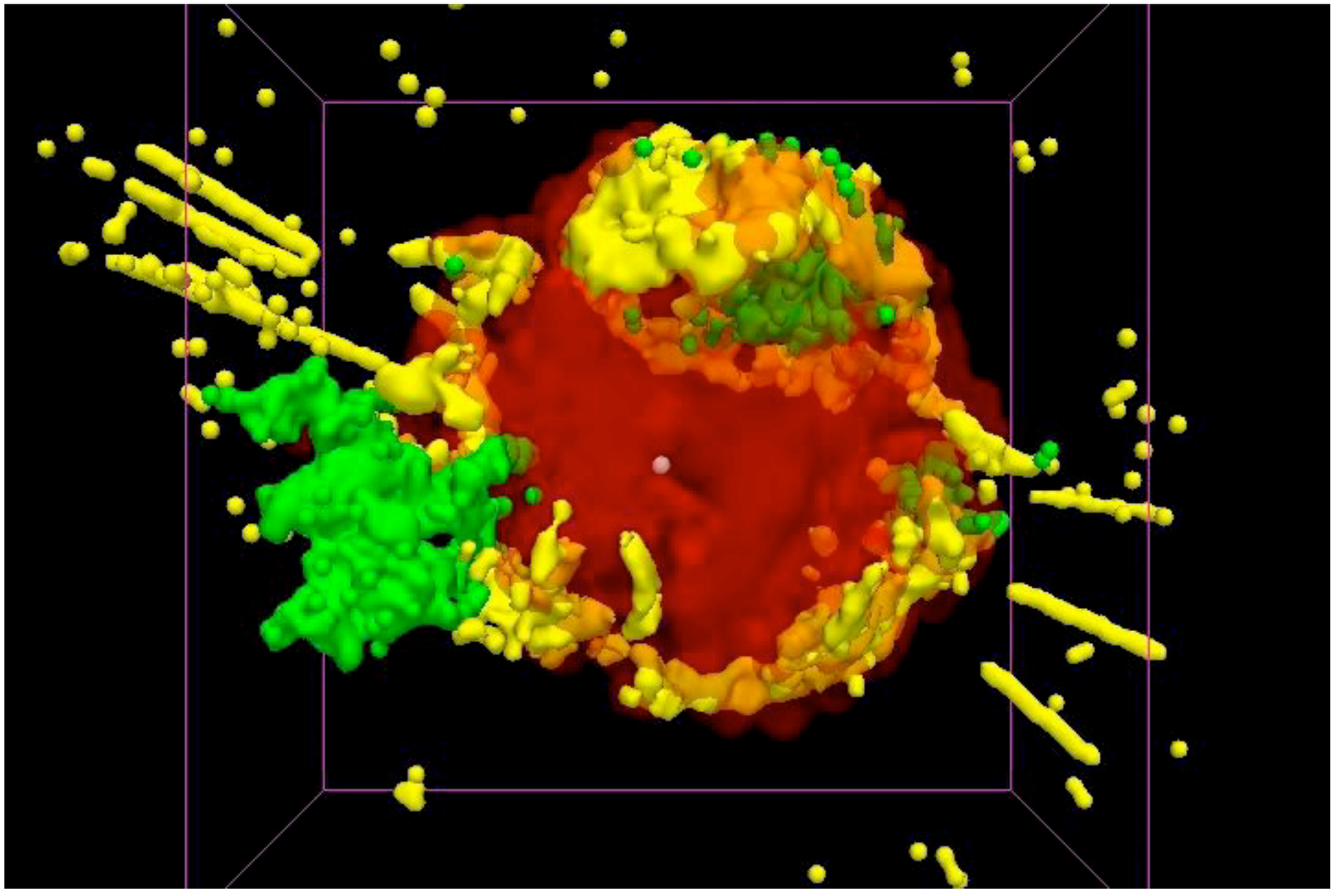

Summary

We discussed s and r-process: s-process produces stable isotopes (N ~ Z), r-process produces neutron rich isotopes that may decay to more stable isotopes. In s process, abundances are modulated by cross section. In r process, they are modulated by decay times (and stability of nuclei). Both tend to peak toward magic number nuclei (nuclei with closed shells for nucleons).

Wolf Rayet Stars are massive stars with bright Helium emission lines, and often bright Carbon, Nitrogen and/or Oxygen emission lines that form in winds. Hydrogen is usually absent.

Luminous Blue Variables (LBV) are undergoing large eruptions, may be intermediate state between Red Supergiants and Wolf Rayet Stars (or not).

Massive stars in these stages undergo supernova when their iron core collapses. The core loses energy due to the photodisintegration of iron and nickel and energy losses from neutrinos. The mass exceeds the Chandrasekhar mass.

The iron core collapses until nuclear repulsion stops the contraction. A bounce occurs, but this does not drive the supernova.

The proto-neutron star then loses 10% of its mass in a neutrino wind (that releases 10^{53} erg)

The neutrino wind heats the surrounding gas. The ensuing convection drives shocks into the surrounding gas and the supernova explosion.

A neutron wind driven by the neutrinos creates the r-process.

Observational properties of supernova were reviewed.

Type II supernova show hydrogen lines: they are core collapse.

Type Ia supernova show no hydrogen lines and SiII absorption. They are thought to be white dwarf supernova.

Type Ib and Ic also show no Hydrogen lines. These are probably core collapse supernvoa that lost their hydrogen rich envelopes in a wind.

Supernova remnants interact with material ejected by the star earlier (SN 1987a)

Supernova remants show spatially different distributions for different elements (example: Cass A)